universität wien

MASTERARBEIT / MASTER'S THESIS

Titel der Masterarbeit / Title of the Master's Thesis

„3D cell proliferation patterns in developing bird limbs"

verfasst von / submitted by

Viola Christina Winkler, BSc

angestrebter akademischer Grad / in partial fulfilment of the requirements for the degree of

Master of Science (MSc)

Wien, 2018 / Vienna 2018

Studienkennzahl lt. Studienblatt / degree programme code as it appears on the student record sheet:	A 066 831
Studienrichtung lt. Studienblatt / degree programme as it appears on the student record sheet:	Masterstudium Zoologie UG2002
Betreut von / Supervisor:	Univ.-Prof. DDr. Gerhard Müller

Ich habe mich bemüht, sämtliche Inhaber der Bildrechte ausfindig zu machen und ihre Zustimmung zur Verwendung der Bilder in dieser Arbeit eingeholt. Sollte dennoch eine Urheberrechtsverletzung bekannt werden, ersuche ich um Meldung bei mir.

Abstract

The development and patterning of the vertebrate limb has been of interest in evolutionary developmental research (EvoDevo) for many years. Cell proliferation, as the main factor in growth and therefore of pattern formation, plays a crucial role in embryogenesis. This project has produced a 3D image data set of proliferating cells in the forelimbs and hindlimbs of chick embryos in a series of developmental stages.

The analyzed stages range from HH18, when limb buds are just visible, up to HH31, when digits are already distinguishable. The data shown correspond well to known cell proliferation patterns, which are mostly based on a few physical sections only. The 3D image data from this thesis enable a more detailed observation, due to the possibilities of virtually rotating and slicing the 3D images.

The image sets will be annotated and open-access published to allow interested researchers to use them for their studies. As this thesis is partly technical in its focus, it also demonstrates a scalable method for generating complete 3D images of whole developing limbs. By using fluorescent EdU (5'-ethynyl-2'-deoxyuridine) chemistry and light sheet fluorescence microscopy, visualization of proliferating cells was achieved at single-cell resolution in whole limbs. Also, tests for possible X-ray dense stains using EdU chemistry were run and give new insights on its possibilities.

The data can be used for cell density and cell count analyses, as is shown in a simple form in this thesis. They also provide a basis to guide future experiments on the limbs, such as manipulations of tissues, as well as testing of hypotheses or predictions. Furthermore, the image data can be used to refine and re-evaluate computer models that simulate limb development, patterning and growth.

Zusammenfassung

Die Embryonalentwicklung von Wirbeltierextremitäten sowie von deren Skelettmustern beschäftigt die evolutionäre Entwicklungsbiologie (EvoDevo) seit vielen Jahren. Zellproliferation spielt eine wesentliche Rolle beim Wachstum von biologischen Strukturen und ist dementsprechend essentiell für die Embryogenese. In dieser Arbeit wurden zu verschiedenen aufeinanderfolgenden Zeitpunkten in der Entwicklung 3D-Aufnahmen von Zellproliferationsmustern in Vorder- und Hinterextremitäten von Hühnerembryonen gemacht.

Die analysierten Entwicklungsstadien reichen von HH18 – dem Stadium, in welchem Extremitäten gerade sichtbar werden – bis zu HH31 – in dem bereits die Finger beziehungsweise Zehen unterscheidbar sind. Die produzierten Datensätze stimmen gut mit bekannten Beschreibungen von Zellteilungsmustern in Extremitäten, welche in den meisten Fällen auf wenigen histologischen Schnitten basieren, überein. Dies zeigt, dass die gewählte Methode Zellproliferation zuverlässig darstellt. Die 3D-Bilder aus dieser Arbeit ermöglichen es, die Extremitäten virtuell zu schneiden und zu rotieren um eine detaillierte Beschreibung der auftretenden Muster zu erreichen.

Die produzierten und mit Informationen zum Bildmaterial versehenen Datensätze werden interessierten Wissenschaftlern und Wissenschaftlerinnen durch eine Open-Access-Publikation zugänglich gemacht. Diese Arbeit zeichnet sich durch ihren technischen Fokus aus, da wir zusätzlich zu den 3D-Bilddaten auch eine Methode erläutern, welche das Darstellen von Zellproliferation in 3D ermöglicht und dies mit einer Auflösung, die das Unterscheiden einzelner Zellen zulässt. Diese Methode basiert auf dem Markieren von sich teilenden Zellen mit fluoreszierender EdU-(5’-ethynyl-2’-desoxyuridin)-Chemie und der Verwendung eines Lichtscheibenfluoreszenzmikroskops. Es wurde außerdem getestet, ob mit Hilfe von EdU auch eine Röntgendichte Färbemethode von teilenden Zellen erzielt werden kann.

Basierend auf den nun vorhandenen 3D-Bilderdatensätzen können Zelldichten sowie die Anzahl der sich teilenden Zellen innerhalb der Extremitäten gemessen werden. Dies wurde

auch anhand einer vereinfachten Methode gezeigt. Außerdem bietet sich die Möglichkeit, zukünftige Experimente an Extremitäten – wie zum Beispiel das Manipulieren von Entwicklungsvorgängen oder auch das Testen von Hypothesen und Prognosen – genauer zu planen, da nun nachvollziehbar ist, wann und wo sich Zellen teilen und damit zum Wachstum beitragen. Eine weitere Verwendung liegt darin, dass bestehende computergestützte Modelle und Simulationen von Extremitätenentwicklung und -wachstum sowie von deren axialen Mustern angepasst und neu ausgewertet werden können.

Acknowledgments

First and foremost, I would like to thank Dr. Brian Metscher, without whom this thesis would not have been possible. I am grateful for all the guidance and support I received from him in the course of this work. I also wish to thank Univ.-Prof. DDr. Gerd Müller for providing his perspective on the research and giving useful feedback. I am furthermore grateful to Dr. Igor Adameyko and Dr. Julian Petersen from the Brain Research Center of the Medical University in Vienna for showing me how to use their light sheet imaging system and enabling me to image my samples. To my colleagues at the Department of Theoretical Biology, I am thankful for the engaging scientific discussions and for their general support during this thesis. I would also like to thank Florian, Benedikt and my father for taking the time to proofread this thesis. Finally, I am grateful to Maria for reminding me how the German language works and to Benny, Anni, Björn and Agnetha for keeping me sane during the writing-up period.

Introduction

The growth and development of vertebrate limbs have been of interest in evolutionary developmental biology (EvoDevo) research for many years (Bénazet & Zeller, 2009; Müller, 2007; Shubin et al., 1997; Tickle & Eichele, 1994; Towers, 2018). The questions of which mechanisms lead to a certain pattern of final skeletal structures and digit patterns, and also of how they have changed in evolution has led to different hypotheses and computer models (see e.g. Glimm et al., 2014; Green & Sharpe, 2015; Hentschel et al., 2004; Marin-Riera et al., 2016). Where and when cells proliferate - together with cell death, migration and adhesion - has an especially important influence on the characteristic shape and growth of the developing limb (Ede et al., 1975; Fernández-Terán et al., 2006; Hornbruch & Wolpert, 1970). Cell proliferation is furthermore an important factor in the developing limb's gain of mass (Ede et al., 1975).

The development of limbs in vertebrates starts with limb buds at specific somite positions along the embryonic axis. The bud consists of mesenchymal cells that are surrounded by ectoderm (Bénazet & Zeller, 2009). Limbs are three-dimensional structures and develop differently along the three spatial axes: anteroposterior (AP), dorsoventral (DV) and proximodistal (PD). Tetrapods show a wide variety of limb morphologies. However, an underlying bauplan is conserved and allows for identifying elements, and comparison between species (Shubin et al., 1997).

Vertebrate Limb Development

After the limb buds emerge, they grow along the PD axis. Later they flatten along the DV axis and widen at the distal end. The pattern of the skeletal elements in the limb starts proximally and proceeds distally. The mesenchymal cells in the limbs will condense during development and differentiate into cartilage, and then bone (Niswander, 2003). The skeletal bauplan of the tetrapod limb consists of three parts: the stylopod or upper limb, the zeugopod or lower limb and most distally the autopod or hand/foot. The humerus in the forelimb and femur in the hindlimb form the stylopod and attach to the shoulder or pelvic girdle. The zeugopod consists of two long bones. In the forelimbs these bones are the radius and ulna, and in the hindlimb the tibia and fibula. The third element, the autopod, can be

further divided into the proximal mesopod and a distal acropod. The latter is formed by several bones: the metacarpals in the hand and metatarsals in the foot, as well as the digits. The mesopod is formed by the carpus in the forelimb, and tarsus in the hindlimb (Wagner & Chiu, 2001).In the chick embryo, the patterning of these bones, i.e. the formation of the cartilage primordia, is completed over a timespan of about four days in development, and is visible after about seven days of incubation (Newman & Frisch, 1979).

The apical ectodermal ridge (AER) plays a crucial role in the growth and elongation of the limb during development (Fallon et al., 1994). It is situated at the distal end of the developing limb and appears as an AP-oriented ridge - as the name already implies - along the tip, which forms due to the thickening of ectodermal cells (Wagner & Chiu, 2001). The AER expresses several fibroblast growth factors (FGFs), which are relevant during embryogenesis. For example, FGF8 and FGF10 play a vital role in the formation of the AER, as well as in the initiation of the limb themselves (Kawakami et al., 2001). Experimental manipulations of the AER or FGF result in deformed limbs, which confirms their important role during embryogenesis (see e.g. Saunders, 1984; Sun et al., 2002). Another zone that is important in limb development is the zone of polarizing activity (ZPA). It consists of mesenchyme and is related to the AP axis signaling in the limb. This zone is situated at the posterior margin of the limb. Transplanting the ZPA to the anterior side of the limb will result in a duplication of some or all digits (Tickle et al., 1975). The morphogen active within the ZPA is Sonic Hedgehog (Shh), which was confirmed in experimental studies (see e.g. Drossopoulou et al., 2000; Tickle & Towers, 2017).

Over the years, different models have been described to explain the skeletal and general growth patterns, as well as axis determination in limbs. In the following, one pattern, namely the Turing pattern, will be shortly described, as it is often named as a model for skeletal and digit patterning.

Turing (1952) described a system that can result in different patterns, based on the reaction between chemical substances, so-called morphogens. These patterns emerge spontaneously and with some kind of periodicity. Turing and Turing-like patterns have been found in several organisms by now, for example, in the skin patterns of some fish (Kondo,

2009). Newman and Frisch (1979) presented a model based on the work by Turing, to explain the PD sequence of developing skeletal elements in the wing bud of chick embryos. They concluded that both the AER and possibly fibronectin, a cell surface protein, play crucial roles in establishing the reaction-diffusion system needed to form the pattern. The described model starts with one stripe of precartilage condensation (humerus), followed by a two-element row (ulna and radius) and ultimately the formation of three elements (the three digits in the avian forelimb) (Newman & Frisch, 1979). Later it was shown that by adjusting the original models not only the skeletal wing bud patterns in chick embryos can be explained by reaction-diffusion systems, but also the patterns emerging in mutant chick embryos, as well as in fossils (e.g. Brachupterygius or Sauripterus; Zhu et al., 2010). The basis for these adjustments in the model were studies on chondrogenesis, as well the local autoactivation-lateral inhibition (LALI) framework, suggested by Meinhardt (2008), as mentioned in (Zhu et al., 2010). The LALI system, as opposed to the former understanding of reaction-diffusion models, also includes cellular reactors, in contrast to simple chemical reactions (Zhu et al., 2010). A more recent study suggests that the Turing-like mechanisms observed in digits of vertebrate limb do not actually form stripes, but spaced spots, that elongate later in development (Hiscock et al., 2017).

Signaling and morphogens in developing limbs have been studied extensively (see e.g. Bénazet & Zeller, 2009; Mariani et al., 2017; Yokoyama et al., 2017). Additional knowledge about where and when cells proliferate would lead to a better overall understanding of limb growth and development and would especially guide future experiments on vertebrate limb development.

Previous cell proliferation studies

Even though not everything is yet known about the spatiotemporal distribution of proliferating cells in growing limbs, there are some studies that focused especially on this topic. Previous studies mainly relied on physical sectioning and 2D projection images of limb buds. This fails to provide a complete picture of the developing limb, as it is a three-dimensional structure and therefore should be studied in 3D. The studies introduced in this

section focus on chick limb development, and the stages mentioned follow the staging done by (Hamburger & Hamilton, 1951).

Hornbruch and Wolpert (1970) did one of the first quantitative studies on mitosis during limb bud growth, stating three questions about the development and growth of early limb buds. First, what starts the early outgrowth? Second, how is the paddle shape of the limb determined? And third, how do cell growth and the PD specification of regions relate to one another? This shows that cell proliferation has been a topic of interest for several decades. They note an overall high mitotic index in the mesenchyme at stage HH18 with about 10 percent and a drop to around 2 percent at stage HH30 (Hornbruch & Wolpert, 1970). The mitotic index refers to the percentage of cells in the phase of mitosis. Also a lower overall mitotic index of the ectoderm was observed in the latter stage and explained by the volume-to-surface ratio of the growing limb (Hornbruch & Wolpert, 1970). They also observe no difference in mitotic index of the proximal and distal end between the stages HH18 and HH23, but a decrease in the proximal area at the stages HH24 to HH30. There are some exceptions to this overall pattern at the stages HH21 to HH24, where some regions show a high mitotic index, for example the elbow or wrist. Furthermore, the area of the ulna, radius, wrist and hand seams to grow faster than the humerus region (Hornbruch & Wolpert, 1970).

Ede and colleagues (1975) named cell proliferation by mitosis the most important factor when it comes to the production of a complex structure as the vertebrate limb. They looked at chick embryos at the stages HH24, HH25 and HH27, and found that in these stages a gradient of cell proliferation is visible, with a higher level at the distal tip. They also noted that the gradient in the mitotic cell count drops rather sharply close to the distal tip, and then becomes more gradual. They observed less cell proliferation in stage HH27 compared to stage HH25. In these two stages also a peripheral count was conducted. Stage HH25 showed a gradient from high levels distally to lower levels proximally, which was not observed at stage HH27. More notable is a drop in overall mitoses in the central region between the stages HH25 and HH27 (Ede et al., 1975). In regions of forming cartilage, irregularities in the count of mitotic cells were mentioned. For example, there seems to be a notably lower mitotic level in the region between the forming radius and ulna at stage

HH25. This drop on the count is explained by a correspondence to the region of the 'opaque patch' (OP), a region of cell apoptosis, which will later disappear again (Ede et al., 1975; Hinchliffe & Thorogood, 1974). It is also worth mentioning that there was no significant correlation of mitotic index with cell density at the periphery, but a high correlation along the center of the PD axis of the developing limb (Ede et al., 1975). They concluded that chondrogenesis, which starts with the more proximal elements and then spreads further distally, goes along with less cell proliferation, but a higher density of cells. Areas of cartilage differentiation result in an abrupt fall in the mitotic index, compared to a rise when leaving these areas again (Ede et al., 1975).

The areas of higher cell density, that go along with a drop in mitotic activity, correspond well to precartilage condensations. Therefore these condensations are not due to more cell proliferation, but result more likely from cell movement (Ede et al., 1975).

Both studies described similar patterns when it comes to proliferating cells, especially a higher mitotic index distally compared to proximally. The study by Hornbruch and Wolpert (1970) looked at 11 different developmental stages, but only focused on a medial section and two additional sections above and below. The second study by Ede and colleagues (1975) looked at three different stages and again at a few sections only. Both investigated the wing bud only and did not look at cell proliferation in the developing leg.

A more recent study by Fernández-Terán and colleagues (2006) looked at both cell apoptosis and cell proliferation in developing chick and mouse limbs. In terms of cell death in the chick wing bud four main zones have been described in the past, namely the anterior necrotic zone (ANZ) near the anterior margin of the developing limb, the posterior necrotic zone (PNZ) near the posterior margin, the already mentioned opaque patch in the center, and the interdigital necrotic zones (INZ) between the developing digits (Fernández-Terán et al., 2006). They found that up to stage HH21 cell death was not detectable by using the terminal deoxynucleotidyl transferase-mediated deoxyuridinetriphosphate nick end-labeling (TUNEL) assay (Zakeri et al., 1993). At stage HH21 in the wing and HH22 in the leg, the ANZ was detectable, and continues in the stages HH22 and HH23 in the wing, and up to stage HH28 in the leg, without extending distally past the anterior end of the AER (Fernández-

Terán et al., 2006). In the following stages the ANZ declined. At the stages HH25 to HH27 cell death was seen anteriorly between the zeugopod and autopod in the wing. Also the OP was detected in the center of the limbs from stage HH22 up to stage HH26 in the wing, and from stage HH23 up to stage HH26 in the leg. From stage HH24 on the OP was mostly seen in the developing zeugopod, between the developing radius and ulna in the wing, and between the fibula and tibula in the leg. By stage HH27 the OP is generally not visible anymore.

Also the PNZ was detected in the wing at the posterior border of the limb bud, starting at stage HH23, with a peak at stage HH24 and up to early stage HH26 (Fernández-Terán et al., 2006; Saunders et al., 1962). In the leg the PNZ was detected at stage HH23, but for a shorter time period than in the wing bud, with almost no detectable cells by stage HH24. For both forelimbs and hindlimbs at stages HH28 to at least HH32 cell death was also seen at the posterior margin, proximal to the forming autopod, which was correlated with shaping the limb, but not with the PNZ (Fernández-Terán et al., 2006).

In the wing the INZ began to appear at stage HH29 to HH30 proximal in the space between digit 3 and digit 4. In the following two stages cell death happened extensively in the two interdigital spaces of the forelimb. Also cell death was seen at the anterior border of digit 2 and posterior to digit 4. These are the most anterior and posterior digits, respectively, in the forming wing. In the leg the INZ was first detected between the stages HH29 and HH30, in three interdigital spaces and within them first proximally then distally. The proximal and distal cluster of cell death later becomes a joined region of apoptosis. The INZ declines after a peak at stage HH31 (Fernández-Terán et al., 2006).

In terms of cell proliferation forelimb and hindlimb were described as very similar, beginning with a uniform distribution of mitosis up to stage HH24, with the exception of the areas of cell death described above, which showed noticeably less mitosis. Beginning at stage HH24 fewer cells proliferated in the center of the limb, which corresponds to future chondrogenic regions. They also noted that the distal mesoderm showed many mitotic cells from stage HH27 on. As soon as the digits formed this area of high cell proliferation ended up being just at the tips of the digits up to stage HH31. Thus the interdigital zones showed

no mitosis. Regions of chondrogenesis showed clearly less cell proliferation. If well-defined areas showed less to no cell proliferation, cell death was visible in the same region (Fernández-Terán et al., 2006).

It was also observed that the AER showed cell apoptosis throughout the studied time period from when the AER starts forming. Cell death was uniform along its AP distribution, possibly with a tendency towards anterior, and started before the mesenchyme showed detectable signs of cell apoptosis. Cell death in the ectoderm was restricted to the AER, but cell proliferation was more uniform among the whole ectoderm surrounding the growing limb. This does include the AER where proliferating and apoptotic cells were observed at the same time (Fernández-Terán et al., 2006).

Fernández-Terán and colleagues (2006) gave an overview of several stages in terms of cell death and cell proliferation. They used anti-phosphorylated histone H3 immunohistochemistry to stain sections of limbs for cell proliferation. They looked at sections next to each other and stained either for proliferation or apoptosis. The limb samples were sectioned in the three orthogonal planes. They therefore did look at the pattern in three dimensions but still lack true 3D imaging. Furthermore, the data provided to the reader consists of only two slices for each stages, which makes the images hard to use for further research. Furthermore the focus was more on cell apoptosis (Fernández-Terán et al., 2006).

Ethynyl deoxyuridine (EdU): labeling dividing cells

One way to detect proliferating cells is using EdU (5’-ethynyl-2’-deoxyuridine), which will incorporate into the DNA instead of thymidine during DNA synthesis (Cappella et al., 2008; Chehrehasa et al., 2009; Salic & Mitchison, 2008). This works due to the very similar structure of the two molecules. The advantage of using EdU instead of the former commonly used BrdU (5-bromo-2'-deoxyuridine) is that it is less toxic, more reliable in terms of outcome and can also be used for labeling live cells (Warren et al., 2009).
A copper-catalyzed click reaction (Rostovtsev et al., 2002; Tornøe et al., 2002) results in a covalent bond between the terminal alkyne group of the incorporated EdU and an azide

molecule. By using a fluorophore-conjugated azide molecule in the reaction, detection using for example fluorescence or light sheet microscopy is possible (Figure 1). The use of the click reaction enables detection of the incorporated EdU without the need to denature the DNA first (by using either heat or acid treatment), as would be needed when using BrdU (Warren et al., 2009).

In this study chick embryos were used as a study species. Even though EdU labeling is mostly used on sections of biological samples, a study by Warren and colleagues (2009) showed that EdU resulted in good and time efficient staining of whole mount chick embryos up to stage HH18 using a fluorophore-conjugated azide. In this work we studied chick embryos up to stage HH31. We also tried to establish a protocol to adapt the EdU detection for other imaging techniques.

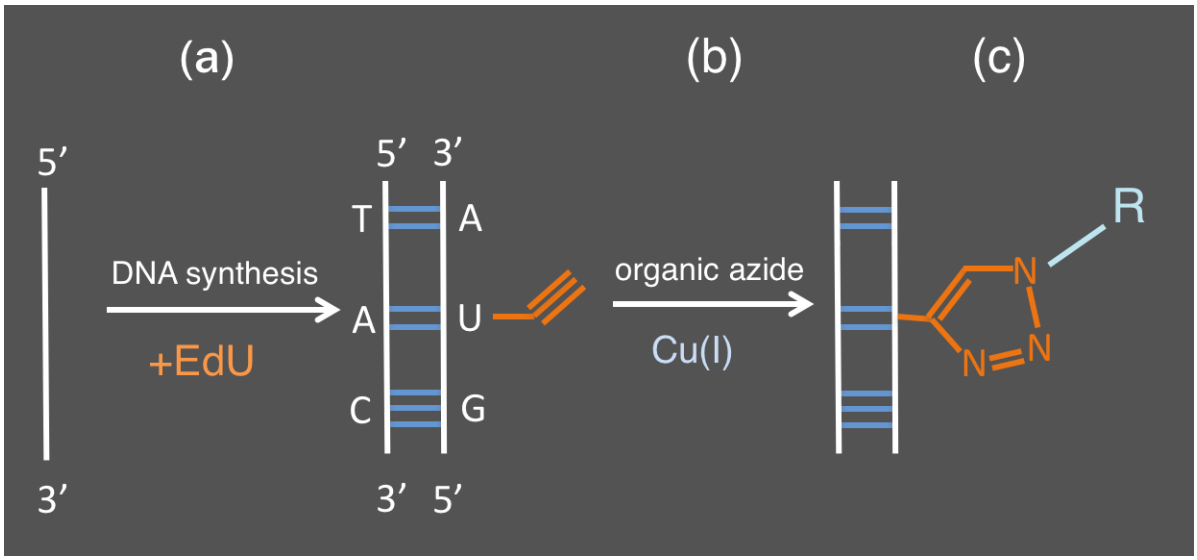

Figure 1 *EdU gets incorporated into the DNA during synthesis instead of thymidine (a). This will lead to an available alkyne group than can be used for attaching an azide during a copper-catalyzed click reaction (b). As a result, the group conjugated to the azide (R) will be attached to the DNA that had EdU incorporated (c). After Cappella et al. (2008) and Salic & Mitchison (2008).*

3D Imaging techniques

Visualization of biological samples is widely employed to reach a better understanding of certain processes or structures. To get a good overall impression of those, a three-dimensional (3D) representation is advantageous, and can be especially helpful in the field

of developmental biology. A 3D image will for example allow for rotating, virtual slicing and segmentation of subvolumes.

Ultimately, a 3D representation using suitable microscopic techniques will result in a number of two-dimensional (2D) images that can be aligned and stacked. This can be achieved by sectioning the used samples and taking pictures of each section. Of course this is a very destructive method. Here we wanted to use a method that is not in need of physical sectioning the samples.

X-ray Microtomography (microCT)

X-ray microtomography is a nondestructive method to get a 3D representation of biological samples. By using X-rays on a rotating sample and a stationary detector many projection images of a sample can be produced. There are also systems available using the clinical CT setup of a stationary sample and a rotating X-ray source and detector. This is very convenient for live samples. By using appropriate algorithms, cross-sections can be calculated from the projection images. X-rays are good for visualizing hard tissues like bones or teeth. Soft tissues can be visualized as well by using metal containing stains (Metscher, 2009).

As we want to visualize cell proliferation, we need a stain specific for dividing cells. By using EdU labeling it was tried to produce a staining protocol that will lead to an accumulation of metal at EdU sites. Molecule-specific staining for microCT has been shown to work (e.g. Metscher & Müller, 2011), but is not well established yet.

Fluorescence Microscopy

Fluorescence microscopy is similar to light microscopy, except that it uses fluorescence or phosphorescence to create an image, instead of absorption and reflection. Usually a high power LED lamp is used as a light source and by using different filter sets the microscope can be adapted to image the used fluorophores. These fluorophores will be excited by the light beam and emit light of a lower wavelength. This light can be imaged using a detector.

This setup does not allow for 3D imaging as described above, but might still give an overview of samples before mounting them for a different imaging system. It can also be used to confirm the presence of fluorophores, even though the samples should not be illuminated too long to avoid photobleaching.

Confocal Laser Scanning Microscopy (CLSM)

Confocal laser scanning microscopy (CLSM) uses optical sectioning to reconstruct 3D structures. It is one type of fluorescence microscopy used to create image stacks of both live and fixed biological samples. This is done by illuminating the sample up to a certain plane, but only focus on that particular plane when taking a picture. A focused light beam scans over the current plane in focus, illuminating small areas one at a time. If a fluorophore is present, it will emit light which will be collected by the objective. If the whole sample (or the area of interest) is fully scanned this way, either the light beam or the sample can be moved vertically to scan other sections at different heights. If all the images are acquired, software can be used to align the pictures and create a 3D representation of the sample.
CLSM gives a quite good spatial resolution and is able to detect single fluorophore molecules. But it does come with a few limitations. By illuminating not just the plane in focus, but the whole sample down to that certain plane, unwanted signal from excited fluorophores from planes out of focus might be detected. Furthermore, even with clearing of the sample – meaning the process of making tissues more transparent and with that allowing the light to penetrate the sample better – only a sample thickness of 100µm to a maximum of 200µm is possible (see e.g. Jonkman & Brown, 2015; Wang & Larina, 2017). In this study the interest was in chick embryo limbs which will be bigger than this limit even early in development. A possibility to overcome this issue would be to cut 50µm to 100µm thick sections of the sample, image these sections using CLSM and then aligning the different stacks to get one complete 3D representation. In the end it was decided against using CLSM due to the constraints in sample size.

Light Sheet Fluorescence Microscopy (LSFM)

Light sheet fluorescence microscopy (LSFM) is similar to CLSM, but increases resolution by creating a light sheet, meaning only illuminating the plane that is currently imaged. To make

this possible the illuminated plane is perpendicular to the detection optics. The light sheet can be produced from either one or two sides and will be only up to a few micrometers thick (Figure 2). Depending on the fluorophores in the sample, lasers of different wavelengths are used.

Samples are mounted within a solution-filled chamber. Depending on the solution's refractive index, suitable sample chambers might be used to increase the quality of the images. Mounting of the samples can be done in numerous ways and will depend on the system and adapters present. LSFM is also suitable for live samples as the efficient illumination of the sample reduces stress or damage induced by the lasers. Imaging is fairly fast and it is possible to get down to subcellular resolution.

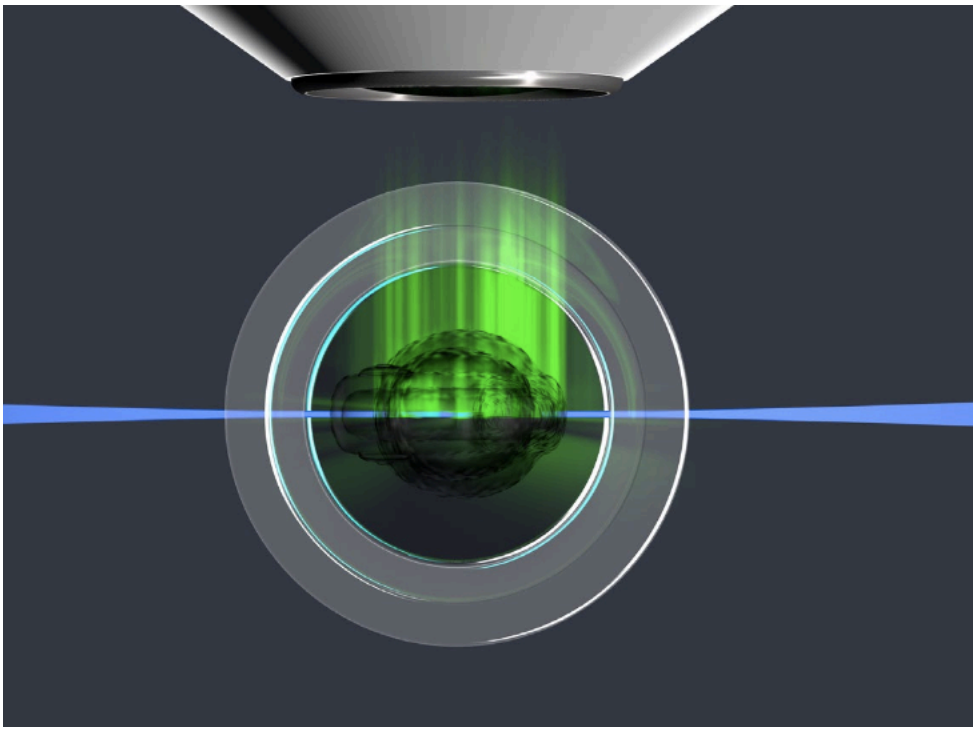

Figure 2 *Illumination of only one plane during imaging using light sheet fluorescence microscopy. The thin illuminated plane (blue) is perpendicular to the detection optics (top) that will image the emitting signal (green) from the fluorophores in the sample. Picture by Zeiss (https://applications.zeiss.com/C125792900358A3F/0/4D1D8D177F06CDF4C1257A940041002D/$FILE/EN_41_011_005_LightsheetZ1_rel2-3.pdf)*

Due to these advantages and a bigger possible sample size than with the CLSM it was decided to image the samples using this method: more specifically with a Zeiss Lightsheet

Z.1 system. Even though imaging of complete chick embryos was not possible, whole limbs of stage HH31 chick embryos could still be imaged without sectioning them first. As in CLSM, clearing of the tissue was needed and samples were mounted in agarose with the help of a syringe (Figure 3). This allowed for very little to no movement of the samples and by that an increase in the quality of the resulted image data.

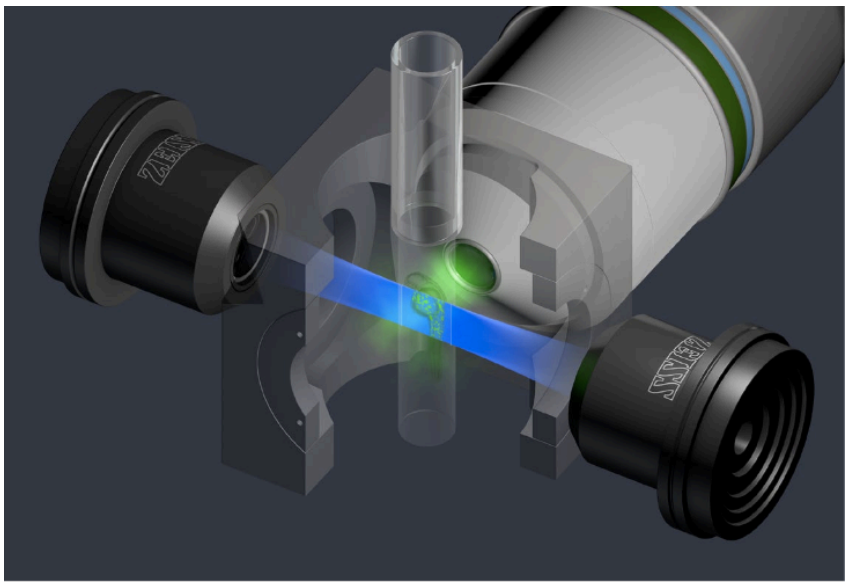

Figure 3 *The light sheet (blue) in the Zeiss Lightsheet Z.1 is created from two sides. The sample is mounted within agarose with the help of a syringe (top) and then lowered into the sample chamber (seen partly in the center of the picture). Excited fluorophores emit light (green) that is then detected by the optics perpendicular to the illuminated plane. Picture by Zeiss (https://applications.zeiss.com/C125792900358A3F/0/4D1D8D177F06CDF4C1257A940041002D/$FILE/EN_41_011_005_LightsheetZ1_rel2-3.pdf)*

Optical Projection Tomography (OPT)

Optical projection tomography (OPT) uses the same principle as X-ray tomography, but uses light instead of X-rays (Sharpe et al., 2002; Sharpe, 2004). OPT can be used for 3D imaging of fluorescent samples. Clearing of the samples is necessary to allow the light to penetrate the sample as needed. This allows samples up to 15mm thick to be imaged (Sharpe, 2002). One big advantage of OPT is that it can be built rather easily, which avoids the need for an expensive commercial setup. Designs for custom built OPT systems are available online for free (see e.g. Wong et al., 2013)

OPT would have been an interesting option to image the samples in our study, even though the resolution would have probably been worse, compared to LSFM. Still, it might have been good enough to get a useful representation of cell proliferation in the developing limbs of chick embryos. Unfortunately, there was no OPT available to image our samples with.

Cell proliferation patterns of developing bird limbs

The aim of this study was to produce 3D images of cell proliferation in whole developing limbs. This work has resulted in a representation of proliferating cells in a series of developmental stages. The resulting patterns were visualized and described. Imaging with LSFM produced in 3D images that can be analyzed at single-cell resolution. Chick embryos were used as a study species due to their easy accessibility as well as their important role as a model species in understanding vertebrate limb development. The data available from this research will allow for correlation of expression patterns and other phenomena in limb development. To enable this, the data will be open-archived and annotated to provide a basis for further research. Furthermore, it was of interest to explore the possibilities of EdU-labeling for imaging techniques requiring X-ray dense stains. A reliable method has not been established, but the work done and shown here contributes to a better understanding of the potential of EdU labeling in that context.

Methods

Specimens

Fertilized chicken eggs were ordered from Schropper GmbH, Gloggnitz, Austria, and incubated in a humidified chamber at 39.4˚C at the Department of Theoretical Biology, University of Vienna. The incubation times were chosen according to Hamburger and Hamilton (1951) and varied depending on the desired developmental stage (Figure 4). We will from now on refer to these stages by adding 'HH' and the assigned numbers by the two authors (e.g. HH21 would stand for developmental stage 21, as describe by Hamburger and Hamilton in 1951). Staging was done after harvesting the embryos and before fixing them in 4% paraformaldehyde (PFA). The main focus for assigning the stages, when in doubt, was on the limb development, rather than other features.

Within the European Union chick embryos can be used in experiments up to day 17 in development without a permission by an ethics committee. The latest stage we used was HH31 and the embryos were incubated for a maximum 6 days and 6 hours.

EdU Labeling of whole-mount chick embryos

Live Embryo Manipulation and Fixation

Eggs were windowed after confirming the position of the embryo within the egg by candling and cleaning the surface with 70% Ethanol. First, a hole was drilled into the base of the egg and about 0.5ml of albumen was drawn out using a syringe. Afterwards transparent tape was put on the shell and a small square window (max. size of 1x1cm) was made through the tape using an ampule file. If possible it was confirmed by sight that the forming heart of the embryo was beating. Then 400µl of 500µM EdU (5'-ethynyl-2'-deoxyuridine) - or 400µl of Phosphate-buffered saline (PBS) in the control group - was added with a pipette on top of the embryo. 500µM is the saturation dose of EdU suggested by Warren and colleagues (2009) and therefore was used in our experiments. Then the window, as well as the hole at the base of the egg was sealed with tape. After windowing the eggs were put back into the incubator for another 4 hours at 39.4˚C before being fixed in 4%PFA in PBS for either 1 hour

at room temperature or over night at 4˚C. There were no differences in outcome due to fixation duration.

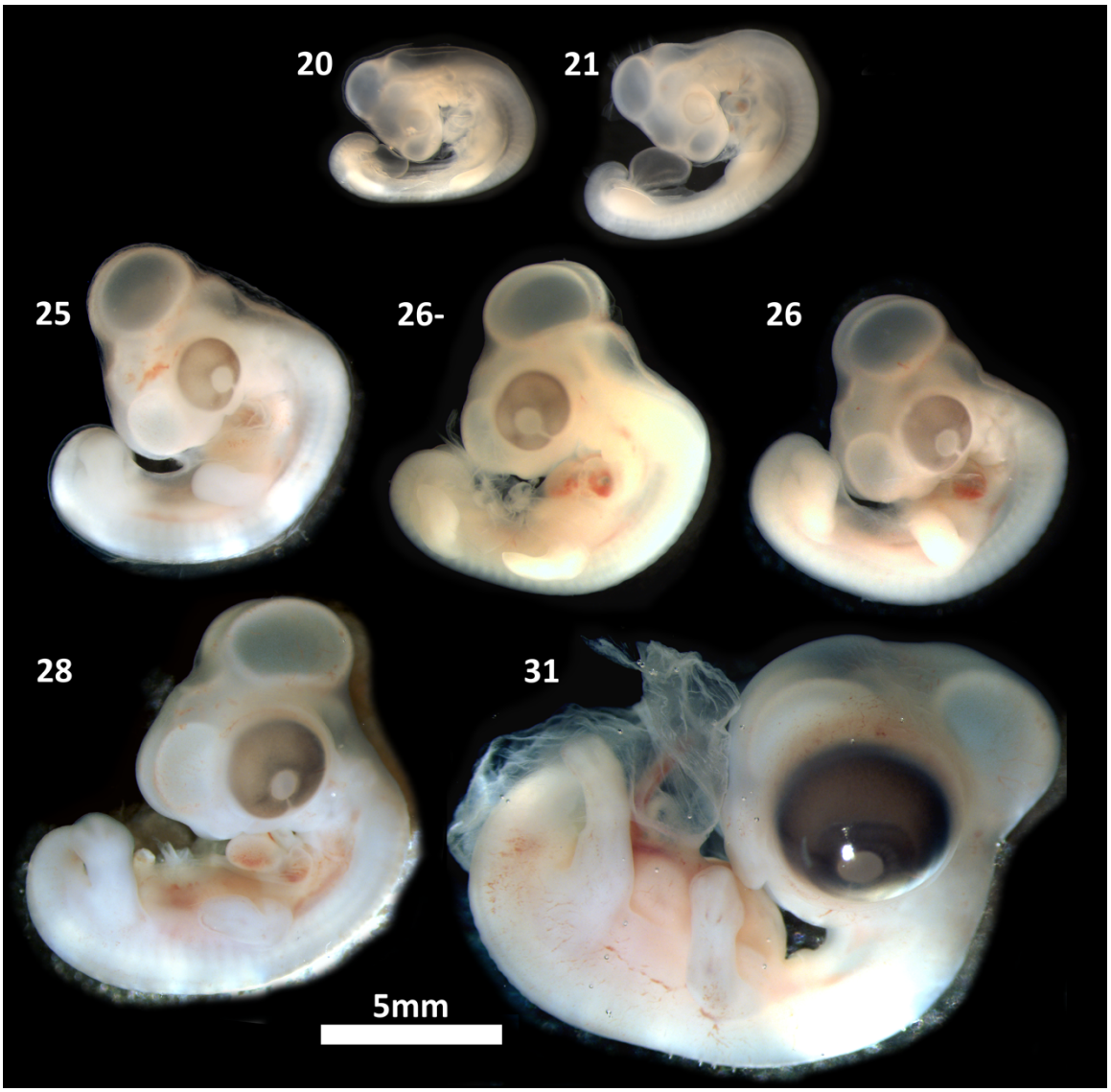

Figure 4 *Scaled pictures of 6 of the 9 chick embryos imaged. The number corresponds to the Hamburger and Hamilton (1951) stage of the specimens. Pictures were taken after fixing the embryos with 4% Paraformaldehyde. Embryos were cut into pieces that fit into the light sheet microscope after taking these overview pictures. This mostly meant cutting of the head and splitting the rest of the body into the upper and lower half. Pictures were obtained using a stereo microscope.*

Fluorescent EdU Chemistry

The idea

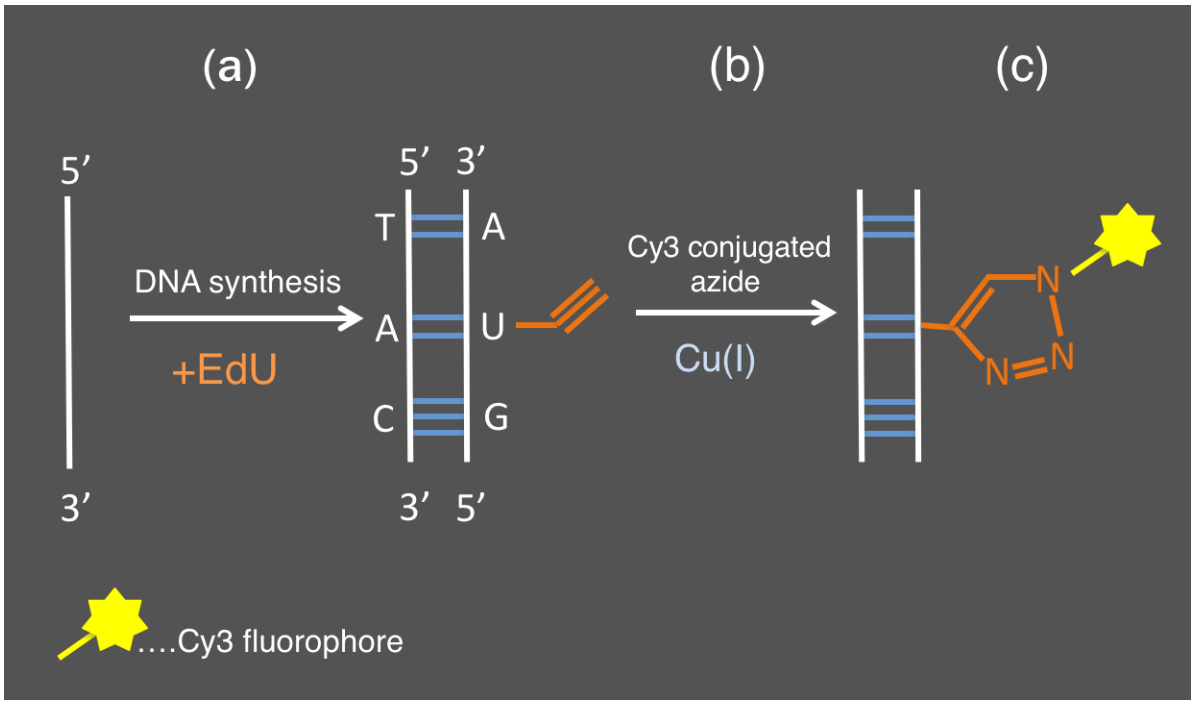

Figure 5 *EdU gets incorporated into the DNA during synthesis instead of thymidine (a). This will lead to an available alkyne group. A Cy3-conjugated azide was attached via a copper-catalyzed click reaction (b). As a result, the fluorophore will be attached to the DNA that had EdU incorporated (c) and can then be visualized using a form of fluorescence microscopy. Cappella et al. (2008) and Salic & Mitchison (2008).*

The principle for fluorescent EdU chemistry was already described in the introduction (see ‘Ethynyl deoxyuridine (EdU) - labeling dividing cells’, page 13). To summarize briefly: EdU gets incorporated into the DNA during synthesis. This will result in available alkyne groups. These alkyne groups can be used to form a covalent bond to an azide via a copper-catalyzed click reaction. Here we used a Sulfo-Cyanine-3-conjugated azide (Figure 5). Cyanine-3 (Cy3) is a well established fluorophore and its excitation maximum was compatible with both the fluorescent light microscope and LSFM used. This method has been used in chick embryo studies before and worked well with our samples (Warren et al., 2009).

Permeabilization

After fixation, samples were rinsed 3 times for 5 min each in PBS. After rinsing in distilled water for 5 min, samples were rinsed twice in 3% BSA in PBS for 5 min each and then

permeabilized for 30 min in 0.5% Triton X-100 in PBS. Next were 3 washes in 3% BSA in PBS for 5 min each.

Labeling of EdU incorporated cells with a fluorophore

The following steps were all done in the dark with the help of a red-filtered LED lamp to avoid excitation of the fluorophores used. An EdU development reagent (100mM TBS; 4mM $CuSO_4$; 2μM Sulfo-cyanin-3 azide, Lumiprobe B1330; 100mM sodium ascorbate) was mixed immediately prior to the application. This reagent contains the components needed for the copper-catalyzed click reaction, as well as the Cy3 fluorophore that was used for visualizing EdU-labeled cell nuclei in this study. The Cy3 used has its excitation maximum at a wavelength of 548nm and its emission maximum at 563nm. The embryo was put into the reagent for 30 min and afterwards rinsed in 3% BSA in PBS for 3 min. It was followed by a rinse in PBS for 5 min, before the embryos were put into a DAPI (4',6-diamidino-2-phenylindole) solution (2μg/ml) for 35 min. DAPI is used as a counterstain as it binds to adenine-thymine rich areas in the DNA and is therefore used as a stain for permeabilized and fixed cell nuclei (Chazotte, 2011). Embryos were again rinsed 3 times in PBS and then stored in fresh PBS at 4˚C.

Signal confirmation

The signals of the fluorophores were first confirmed using a fluorescence microscope (Figure 6) before selected samples – based on the condition of the embryo and signal intensity – were imaged using LSFM (ZEISS Lightsheet Z.1).

To confirm that the Cy3-fluorophore only attached to EdU labeled cells, a control with PBS instead of EdU was run. For these samples, when windowing the eggs instead of 400μl of 500μM EdU, the same amount of PBS was pipetted on top of the embryo. Otherwise the exact same protocol was run. The control samples did not show any Cy3 signal under fluorescent light (Figure 6), which confirms that the Cy3-fluorophore was only attached to EdU labeled DNA.

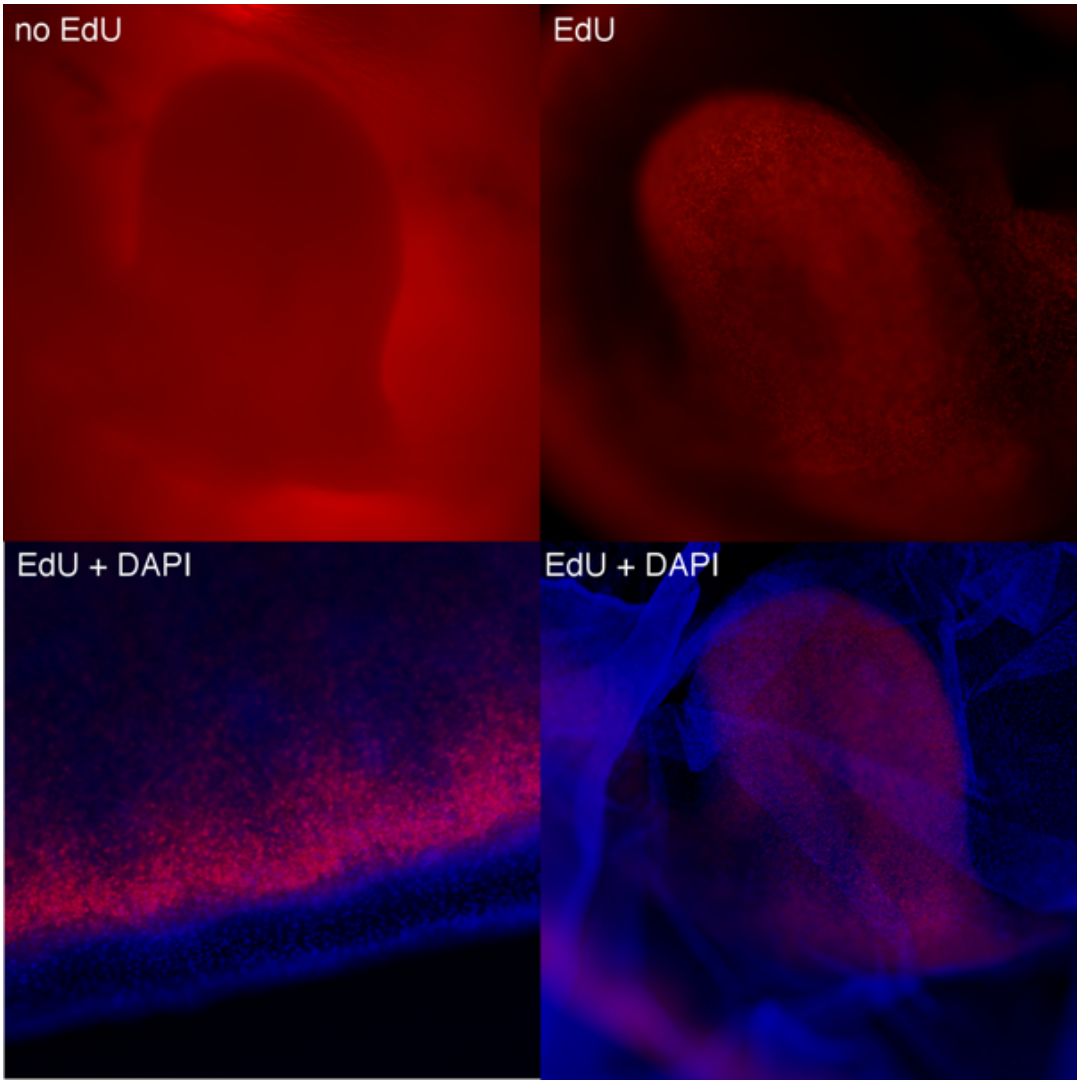

Figure 6 *Top row shows the comparison of a Cy3-EdU (red) stained chicken embryo limb (right) and one limb from the control group, that was not exposed to EdU during development (left). It is clearly shown, that no fluorophore staining is visible in the latter sample, due to the lack of incorporated EdU into the DNA.*
Bottom row shows the back or dorsal side of a chick embryo on the left, and a limb with surrounding membranes on the right. The red dots correspond to the Cy3-EdU labeling and blue areas to the cell nuclei stained with DAPI. Some cell nuclei show staining of both fluorophores as expected.

Silver staining of EdU labeled cells

The idea

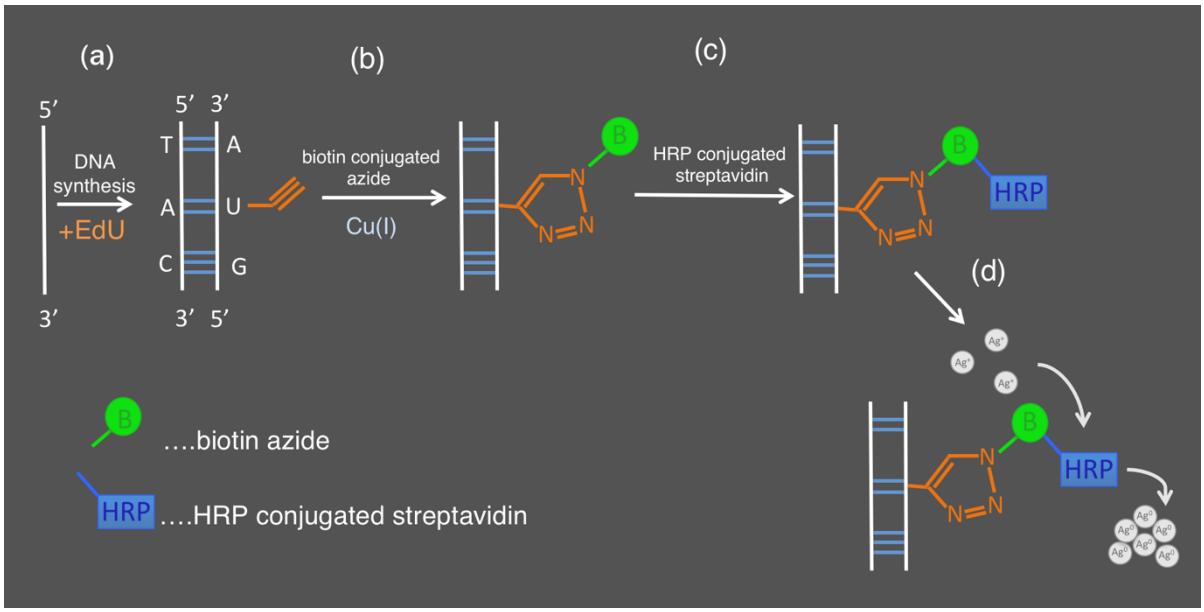

Figure 7 *EdU gets incorporated into the DNA during synthesis instead of thymidine (a). This will lead to an available alkyne group. Here a biotin-conjugated azide via a copper-catalyzed click reaction was attached (b). By adding HRP conjugated streptavidin (streptavidin has a high affinity to biotin), the peroxidase will be bound to the now attached biotin (c). As a next step silver ions are introduced and will ideally be reduced to insoluble metallic silver (d). The silver will therefore be accumulated at EdU labeled sites. Steps (a) und (b) after Cappella et al. (2008) and Salic & Mitchison (2008).*

As mentioned in the introduction microCT is another form of visualizing objects or biological samples in 3D. Early embryonic tissues have little to no X-ray density, which is why staining is needed. For an overall staining of samples phosphotungstic acid (PTA) or Lugol's solution (IKI) can be used to stain soft tissues (Metscher, 2009). Specific staining of certain tissues is much more complicated, but has been shown to be possible (Metscher & Müller, 2011). Based on the work by Metscher and Müller (2011) a protocol was adapted to try to stain EdU labeled cells. The idea was to use the fact that peroxidase will reduce positively charged silver ions (Ag^{+}) to insoluble metallic silver (Ag^{0}). To attach peroxidase to the EdU labeled cells, first a biotin-conjugated azide was connected to the alkyne group of the incorporated EdU. As a next step the samples were exposed to HRP (horseradish peroxidase) conjugated streptavidin. Streptavidin has a strong affinity for biotin and will connect to it if exposed. Thus peroxidase gets attached to the EdU labeled cells. By putting the samples in contact

with silver, we hoped for a reduction of the silver ions to happen and by that an accumulation of silver in the cell nuclei (Figure 7).

Permeabilization

After fixation samples were rinsed 3 times for 5 min each in PBS and then put into 1% hydrogen peroxide for 15 min to inhibit endogenous peroxidase in the samples. After rinsing in distilled water for 5 min, samples were rinsed twice in 3% BSA in PBS and were then permeabilized for 30 min in 0.5% Triton X-100 in PBS. Next were 3 washes in 3% BSA in PBS 5 min each.

Labeling of EdU incorporated cells with silver

An EdU development reagent (100mM TBS; 4mM CuSO4; 4μM Biotin-PEG3 azide, Lumiprobe C3730; 100mM Sodium Ascorbate) was made immediately prior to putting the embryo in it for 30 min. Two rinses in 3% BSA in PBS followed. Samples were then put into a 1:1000 diluted HRP conjugated streptavidin (ThermoFisher N100) solution in 3% BSA in PBS for 3 hours at room temperature on a rocker. Samples were then rinsed in 0.1% saponin in PBS for 5 min, 30 min and over night. It was later observed that exchanging an over night wash to another wash for 30 min is not resulting in different outcomes. Samples then were washed twice with 0.1% Triton X-100 in PBS for 30 min each.

Then a postfixation was done for 20 min using 10% Formalin in 0.1% Triton X-100 in PBS. After three more rinses (5 min each) in distilled water, samples were transferred to fresh tubes to eliminate the presence of salts in the tube. Then equal parts of citrate buffer (0.4M, pH 3.8-4) and silver acetate (4.8mg/ml) solution were added to the sample for 4 min. Next followed a 0.4% hydroquinone solution with the same volume for another 4 min. Then another equal volume of 0.3% hydrogen peroxide was added. As soon as the solution turned gray - caused by precipitating silver - it was exchanged for distilled water and after 3 more washes the embryos were stored in PBS at 4˚C.

The outcomes from this protocol varied greatly. Mostly the silver staining did not seem to be very specific to the cell nuclei (Figure 8a). On the other hand, some areas showed some specific-looking stain that resembled to some degree the expected patterns for cell proliferation, for example, in the limb (Figure 8b).

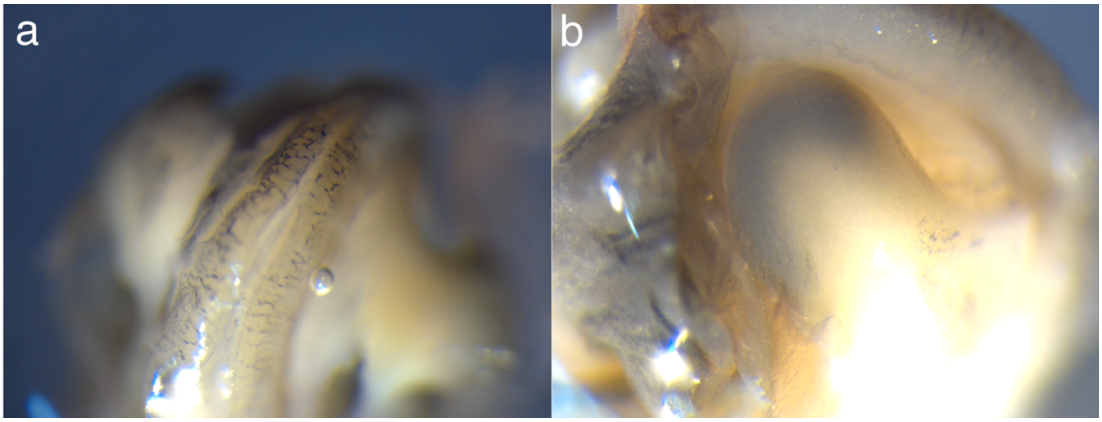

Figure 8 *Chick embryo sample stained with silver. The silver is not very specific and shows unevenly stained parts of the embryo. Some areas of the staining look rather superficial (a), others seemed to stain areas within the embryo, as for example in the limb (b)*

When leaving out the 15 min in 1% hydrogen peroxide after the fixation and washes in PBS, one sample showed specific staining in the cell nuclei (Figure 9). It is not clear though how well the stain penetrated and if only cell nuclei close to the surface of the embryo were stained. Furthermore, it did not store enough silver to be imaged using microCT (results from scan not shown).

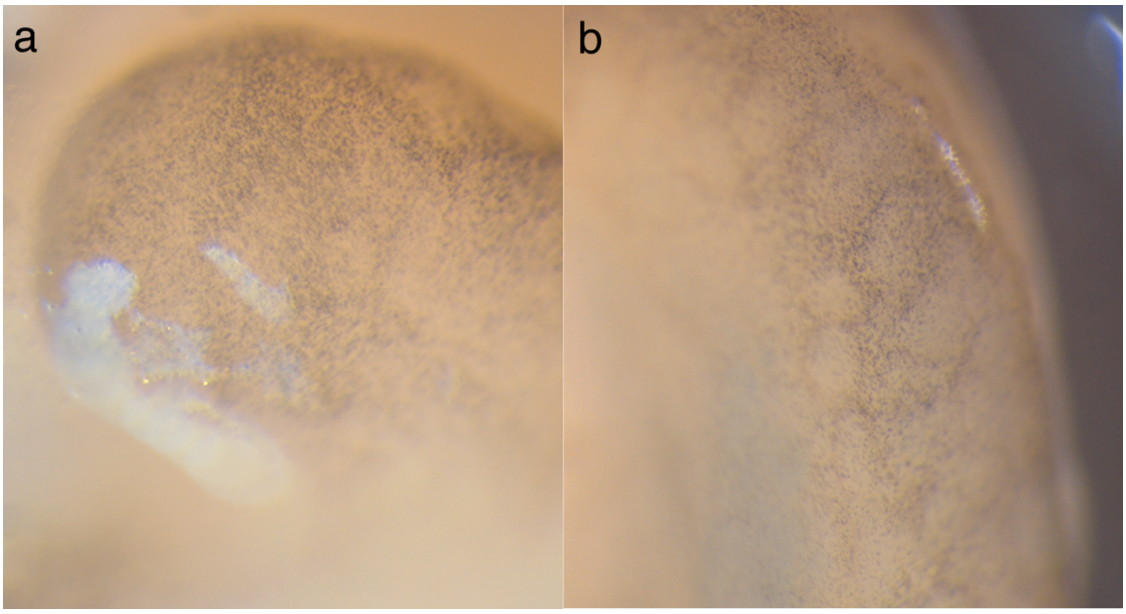

Figure 9 *Chick embryo limbs labeled with EdU and then stained with silver. Both the limb (a) and the back (b) show specific staining of cell nuclei. From the sample it was unclear how well the stain penetrated the tissue.*

Yet another sample showed contrast in X-ray imaging. Here again, the sample was not put into hydrogen peroxide after fixation and there were no washes in 0.1% Triton X-100 in PBS before postfixation. Additionally, a change in color of areas of the embryo, as well as of the solution, was observed after adding the hydroquinone, so no hydrogen peroxide was added in the end, but instead the reaction was stopped by changing the solution to distilled water. It is not completely clear from the X-ray images if the staining is specific to the EdU sites in the embryo, or if the pattern seen results from other sites of staining (Figure 10).

Samples were scanned using the Xradia MicroXCT imaging system (XRadia, Inc., Pleasanton, CA). They were mounted in aqueous agarose within a plastic tube to keep them from moving for the time of scanning.

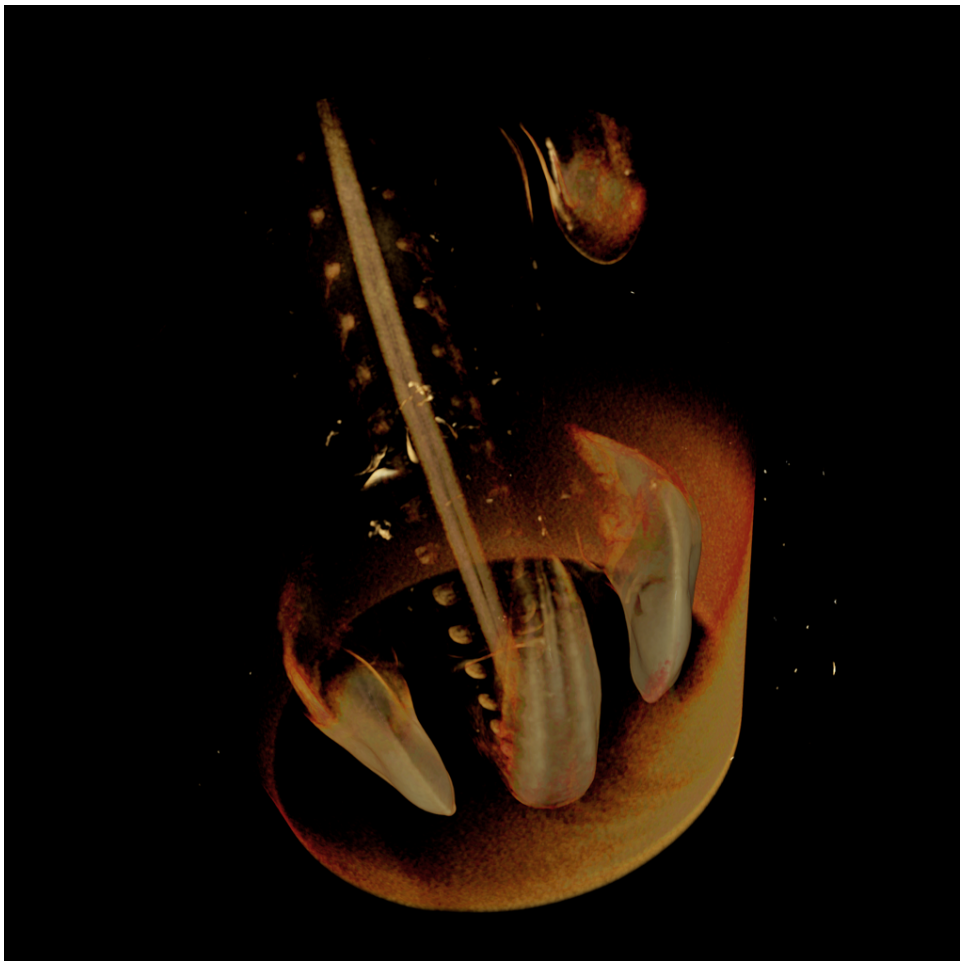

Figure 10 *3D volume rendering based on a microCT scan of a chick embryo possibly showing areas that were labeled with EdU and then stained with silver. Visible are both hindlimbs in the bottom part of the pictures as well as the tail, possibly somites (spots) and the left forelimb (top right).*

DAB Staining of EdU labeled cells

The idea

DAB (3,3'-diaminobenzidine tetrahydro-chloride) is a brown to black stain that is commonly used in histology. Furthermore, metal-enhanced kits exist or poststains involving metals are in use. Here the idea was to get metal into the cells that contain EdU, to possibly produce a specific X-ray dense stain.

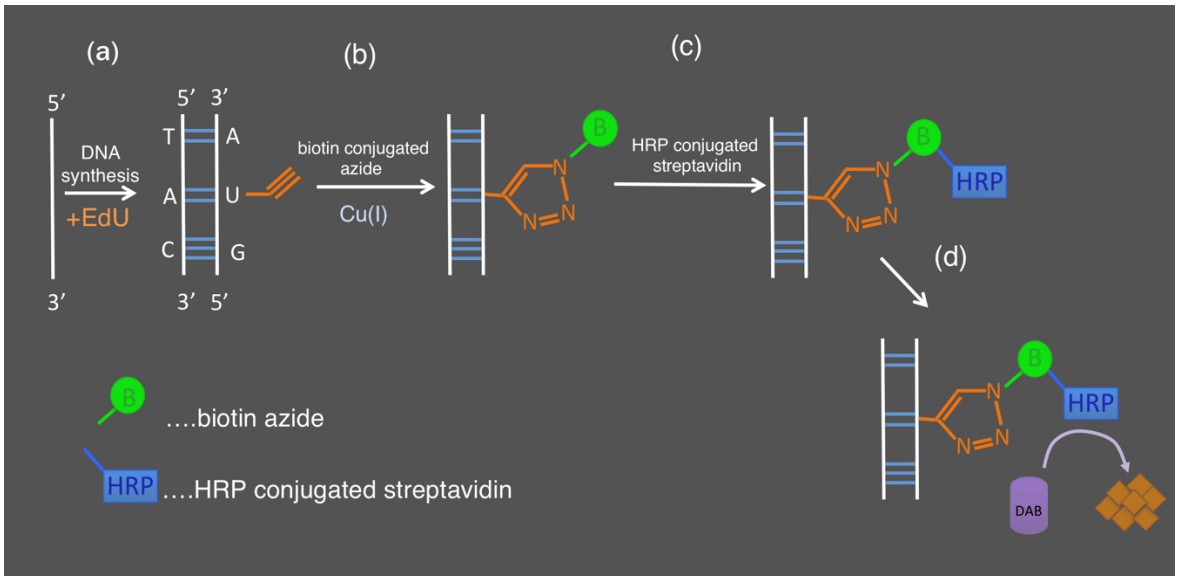

Figure 11 *EdU gets incorporated into the DNA during synthesis instead of thymidine (a). This will lead to an available alkyne group. Here a biotin-conjugated azide via a copper-catalyzed click reaction was attached (b). By adding HRP conjugated streptavidin (streptavidin has a high affinity to biotin), the peroxidase will be bound to the biotin (c). As a next step DAB is introduced and reduced by the peroxidase, which should ideally lead to particles being accumulated in the cell nuclei (d). Steps (a) and (b) after Cappella et al. (2008) and Salic & Mitchison (2008).*

Similar to the staining containing silver - described in the previous section - a biotin-conjugated azide was used and then HRP conjugated streptavidin to ultimately connect peroxidase to the EdU labeled cells. The only difference was that instead of a silver solution a DAB solution is used (Figure 11). Also via a reduction of added metal ions the brown particles should be accumulated in the cell nuclei and allow for detecting EdU labeled cells either by using light microscopy or microCT (in the case of the metal-enhanced DAB). The metal-enhanced DAB kits available (e.g. 34065 Thermo Fisher Metal Enhanced Substrate Kit) use cobalt or nickel, which both are not heavy enough to be visible in microCT scans. Therefore, ultimately a poststain containing a heavier metal might be necessary when using DAB.

Permeabilization

After fixation samples were rinsed 3 times in PBS for 5 min each, and then put into 0.3% hydrogen peroxide in PBS for 5 min, followed by three more 5 min washes in PBS. After 2 rinses for 5 min each in 3% BSA/PBS, samples were permeabilized for 30 min in 0.5% Triton X-100 in PBS. After rinsing twice for 5 min each in 3% BSA/PBS and twice for 5 min in PBS,

samples were put into Proteinase K (20μg/ml) for 20 min. Next followed 3 washes for 5 min each in PBS.

Labeling of EdU incorporated cells with DAB

Samples were put into an EdU developmental reagent (100mM TBS; 4mM CuSO4; 4μM Biotin-PEG3 azide, Lumiprobe C3730; 100mM sodium ascorbate) containing a biotin-conjugated azide. Three more washes 5 min each in PBS followed, before the solution was changed to HRP-conjugated streptavidin (Thermo Fisher N100) in 3% BSA/PBS (diluted 1:1000) for 3 hours on a rocker at room temperature. After rinsing three times in PBS and twice in distilled water, samples were put into a metal enhanced DAB solution (DAB/Metal Concentrate from the 34065 Thermo Fisher Metal Enhanced DAB Substrate in working concentration) until desired staining (usually after 5 to 15 min) was accomplished. To stop the process samples were rinsed in distilled water before storing them at 4˚C.

Results

This protocol led to different results. One sample fell apart after the treatment with Proteinase K, but the protocol was resumed anyway. This sample did show specific staining of cell nuclei, even though no estimation of the penetration of the stain was done (Figure 12a-c). On the other hand, another embryo that was used at the same time, following the exact same protocol, showed no obvious staining of cell nuclei, except for some areas of membranes that were still attached ventrally to the embryo (Figure 12d-e). The only difference observed in the course of the experiment was, that the latter sample floated longer at the top of the used liquids, compared to the first one. But eventually both embryos sank to the bottom of the tubes.

A poststain was not performed due to the varying results. Possible metal candidates to try might be platinum - which has been used in combination with DAB before (see e.g. Hiraoka & Hirai, 1992) – as well as gold or osmium tetroxide (see e.g. Newman et al., 1983)

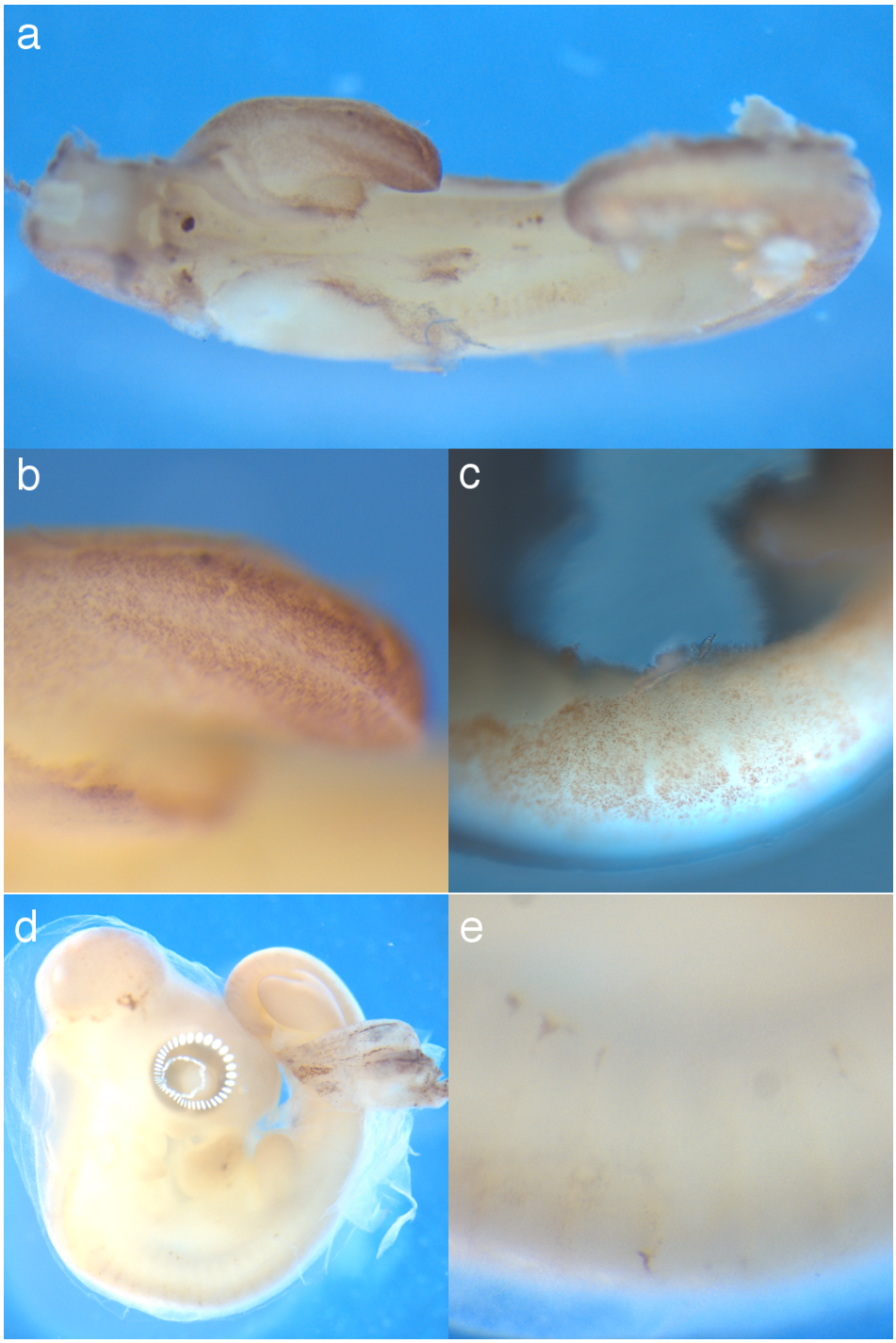

Figure 12 *Chick embryos with EdU labeled cells that were then stained with DAB. (a-c) Sample that showed specific cell nuclei staining, even though penetration seems to be quite bad. (d+e) Sample that went through the same steps as the shown in the pictures a to c, but showed almost no staining at all, beside a few darker areas on the dorsal side of the embryo (e).*

Clearing

Light sheet microscopy requires optically cleared samples. The protocol used was adapted from Susaki and colleagues (2014) and Tainaka and colleagues (2014) and kindly provided by Julian Petersen (Brain Research Center, Medical University Vienna, Vienna, Austria). The clearing protocol relies on a clearing and imaging method, named CUBIC (clear, unobstructed brain imaging cocktails and computational analysis; Susaki et al., 2014). For clearing, samples were first transferred into glass tubes and then put into the first clearing reagent (25% urea; 25% N,N,N',N'-tetrakis(2-hydroxypropyl)ethylenediamine; 15% Triton X-100; all in distilled water) for at least 1 hour at room temperature or at 40˚C by using a heating block. Samples can also be left overnight in the solution. After confirming visually that samples had cleared noticeably, they were switched to PBS for at least two washes of a minimum of 30 min each. Samples were then transferred into the second clearing reagent (50% sucrose; 25% urea; 10% 2,2˚,2˚-nitrilotriethanol; 0.1% Triton X-100; all in distilled water) and left overnight on a rocker at room temperature. Samples were stored in the same reagent at 4˚C until imaged.

3D Imaging: light sheet microscopy

For mounting the samples in the LSFM (Zeiss LightSheet Z.1) it was first tried to glue the samples to a thin string of plastic tube using super glue. As this resulted in damaged samples and uncontrolled movement of the samples during the scan, this method was abandoned. Samples were then exclusively embedded in a syringe using agarose instead. For this, agarose was mixed using distilled water and the second clearing reagent in a ratio of 1:3. The syringe is then put into the light sheet microscope using an adapter that is available for the Zeiss LightSheet Z.1. Samples can be easily lowered into the chamber using the syringe, which will only leave the agarose surrounding the sample (Figure 3). By filling up the chamber with the second clearing reagent shortly afterwards to prevent drying of the sample, mounting is completed. The sample chamber is specific to the refractive index (n=1.45) of the clearing solution, as well as the agarose which increases the quality of the images.

The scan setup is done using ZEN, a software provided by Zeiss and specifically designed for the Lightsheet Z.1. The needed lasers and filters, as well as the area of interest can be selected, as well as parameters like exposure time and the alignment of the lasers. The scans were performed using a multiview setup and the coordinates for the needed tiles were created using LS Tile Scan. When everything is set, the scan will be started and usually only takes a few hours to be completed.

Analysis

The resulting files were loaded into the Arivis Vision4D software for further editing. As two different fluorophores were used (Cy3 and DAPI) there were also two channels from the scan. In Arivis Vision4D the images taken of each plane were stitched and aligned using the Tile Sorter, their brightness adapted and then saved as two TIFF image stacks – one per channel. These stacks were loaded into ImageJ (http://imagej.net) to be transformed into 8-bit images, scaled down and cropped. As the image stacks were huge in data size these steps enabled us to reduce the size sufficiently to allow us to use Amira 6.4 (FEI Visualization Science Group, Burlington, MA, USA) for further analysis. In Amira the stacks could then be displayed as volume renderings and sliced in any direction necessary to get a good impression of the existing cell proliferation patterns in 3D.

The image stacks obtained from the LSFM consisted of grayscale images. These were in most cases later overlaid with colored transfer functions to allow for better representation of the data.

Results

In total scans of seven forelimbs (Figure 13) and eight hindlimbs (Figure 14) of a total of nine different developmental stages were analyzed. Stages range from HH18 to HH31. A minus (‘-‘) was attributed to the stages if the limbs did not yet show all the features of a stage as described by Hamburger and Hamilton (1951), but were clearly distinct from the previous stage.

We will assume in our analysis that the overall size of the embryos does not have an influence on the cell proliferation patterns observed in the samples and described in the following pages.

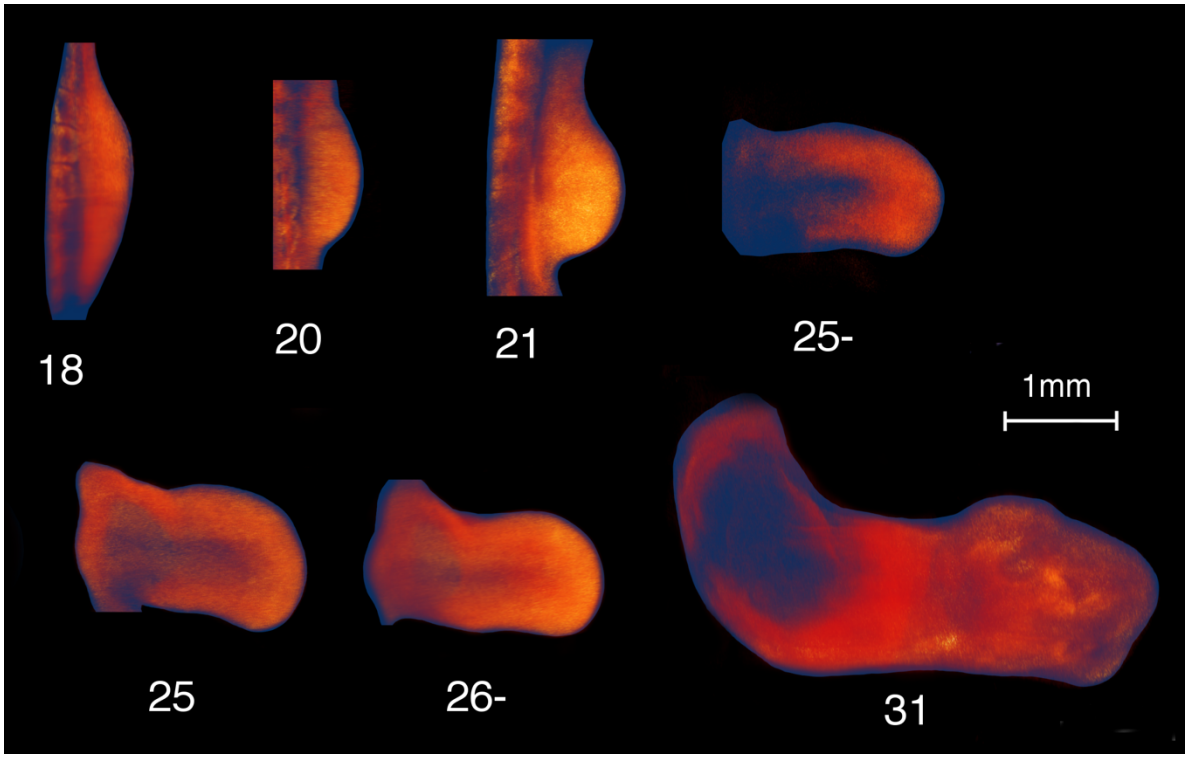

Figure 13 *Scaled 3D volume renderings of all the forelimb samples used in the analysis. Limbs were mirrored to all point in the same direction if needed. Numbers correspond to the Hamburger Hamilton stages of the chick embryos. Red areas represent cells that have incorporated EdU during synthesis and have been stained with Cy3. The blue color represents the outline of the limbs, based on DAPI staining in the sample.*

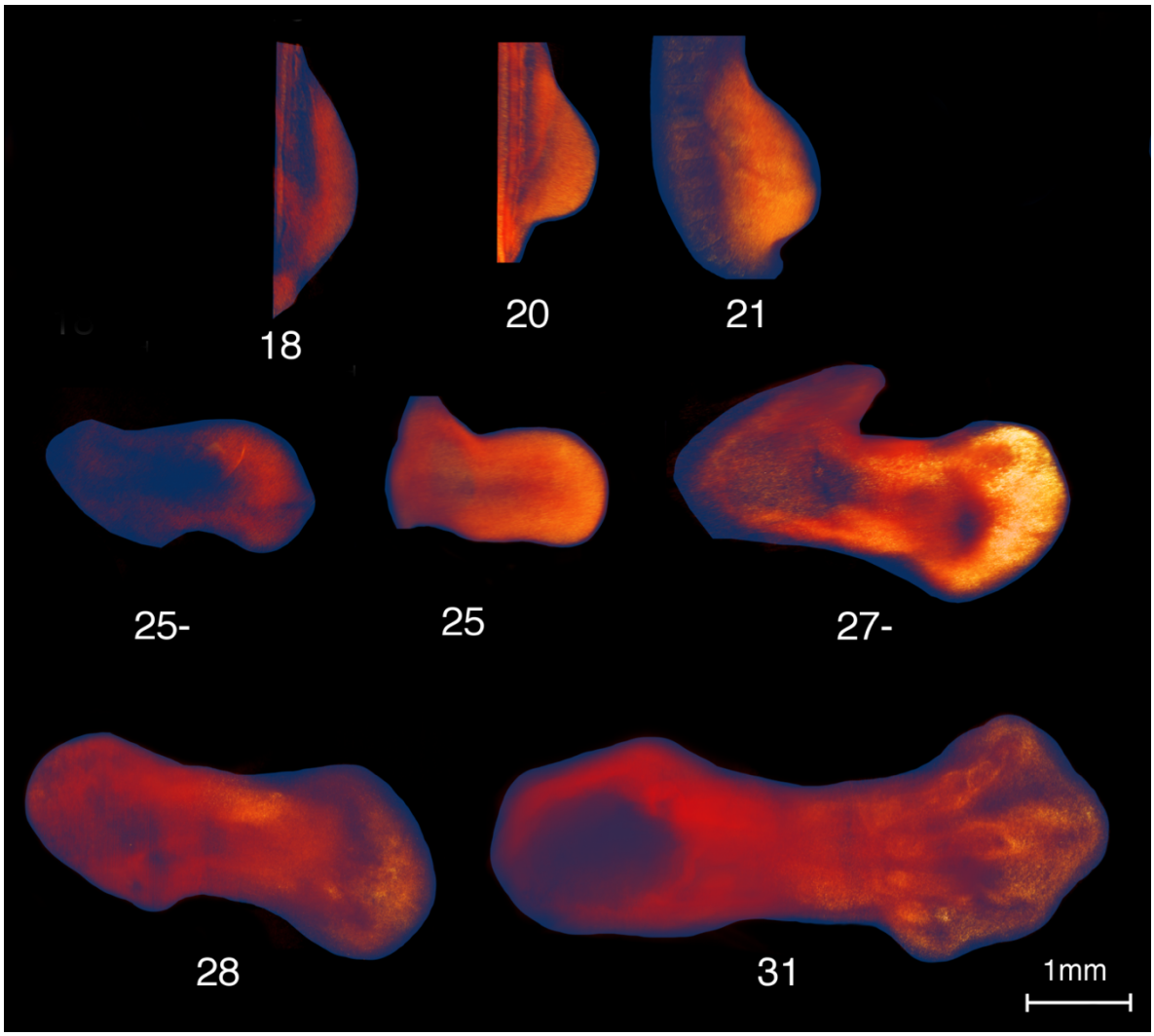

Figure 14 *Scaled 3D volume renderings of the chick embryo hindlimbs used in the analysis. If needed images were mirrored so all limbs point towards the right side. Numbers correspond to the Hamburger Hamilton stages of the chick embryos. Red areas represent cells that have incorporated EdU during synthesis and have been labeled with Cy3. The blue color represents the outline of the limbs, based on DAPI staining in the sample.*

Stage HH18

Forelimbs

Cell proliferation is seen throughout the whole limb, with no clear sign of any differences in density. Proliferation seems to be uniform (Figure 15 andFigure **16**). There are no clear areas where no cell proliferation is happening. On the virtual sections a small border can be seen around the outside of the forelimb, followed by a one-cell-deep layer around it (Figure 15).

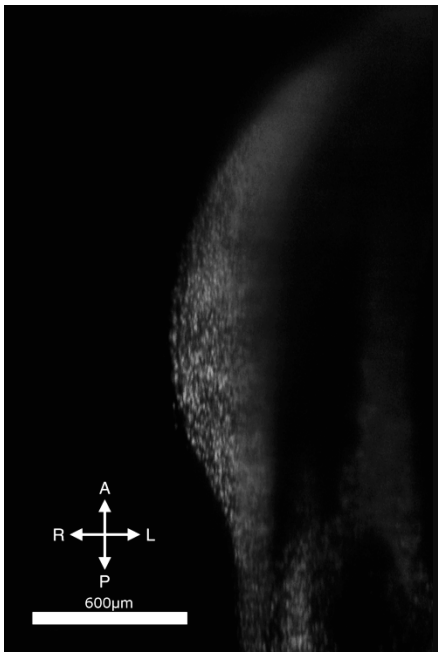

Figure 15 *Virtual section through the right forelimb of a chick embryo at stage HH18. White dots represent cells that have incorporated EdU during synthesis and have been stained with Cy3. A: anterior, P: posterior, R: right, L: left*

Figure 16 *Cross section through a chick embryo at stage HH18, showing sections through both forelimbs. At the top of the picture the spine is visible at the dorsal side of the embryo. White dots represent cells that have incorporated EdU during synthesis and have been stained with Cy3. D: dorsal, V: ventral, R: right, L: left*

Hindlimbs

Similar to the forelimb at the same stage, cell proliferation seems uniform with no distinction between different areas within the limb (Figure 17). There might be slightly less EdU labeled cells at the proximal part of the limb (Figure 19). A small border – a couple of cells thick – can be observed around the outside of the limb (Figure 18).

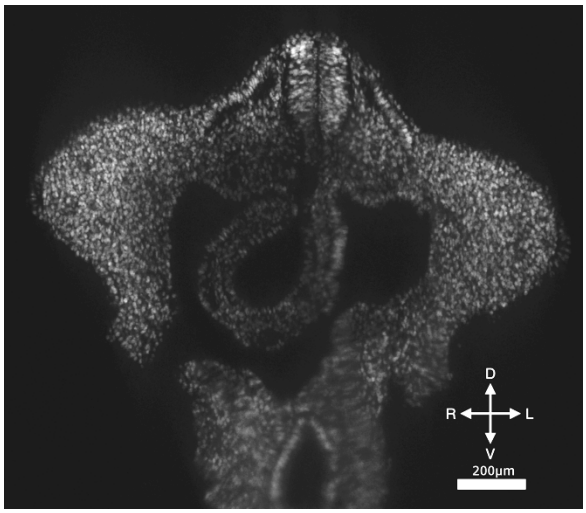

Figure 17 *Virtual cross section through a chick embryo at stage HH18 that shows both hindlimbs on the right and left side. At the top of the image - the dorsal side - the neural tube can be seen. White dots represent cells that have incorporated EdU during synthesis and have been stained with Cy3. D: dorsal, V: ventral, R: right, L: left*

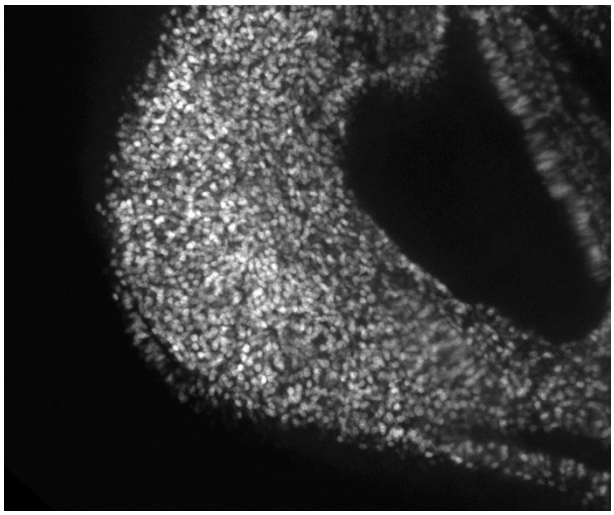

Figure 18 *Close up of a virtual cross section through the right hindlimb of a chick embryo at stage HH18. In this picture a thin layer of cells around the limb is visible. White dots represent cells that have incorporated EdU during synthesis and have been stained with Cy3. The top of the image points dorsally and the left side to the right-wing side of the embryo.*

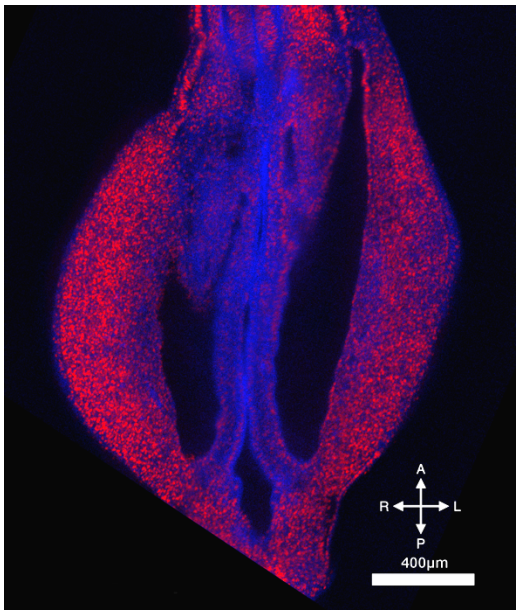

Figure 19 *Virtual dorsal plane through both hindlimbs of a chick embryo at stage HH18. Red dots represent cells that have incorporated EdU during synthesis and have been stained with Cy3. Blue dots show the cell nuclei that were stained with DAPI. A: anterior, P: posterior, R: right, L: left*

Stage HH20

Forelimbs

There are fewer cells proliferating in the center of the limb (Figure 20Figure 21). Besides that, the pattern of cell proliferation seems uniform. On the virtual sections a small border can be seen around the outside of the forelimb, followed by a one cell thick layer around it. The DAPI stain shows an even distribution of cell nuclei throughout the whole limb, which confirms, that the pattern of lesser density in the center of the limb is due to a lower amount of EdU labeled cell nuclei (Figure 21).

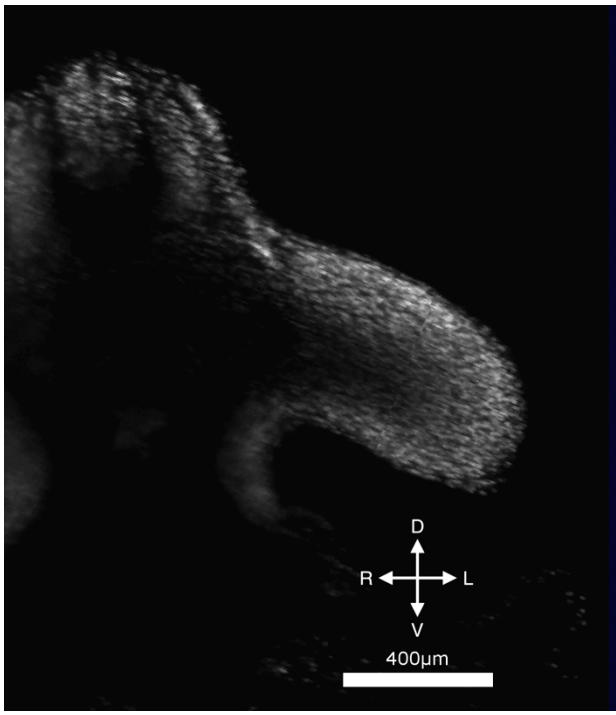

Figure 20 *Virtual cross section through the body and especially left forelimb of a chick embryo at stage HH20. Dorsally the neural tube can be seen. In the limb more cells have been labeled with EdU distally. White dots represent cells that have incorporated EdU during synthesis and have been stained with Cy3.*
D: dorsal, V: ventral, R: right, L: left

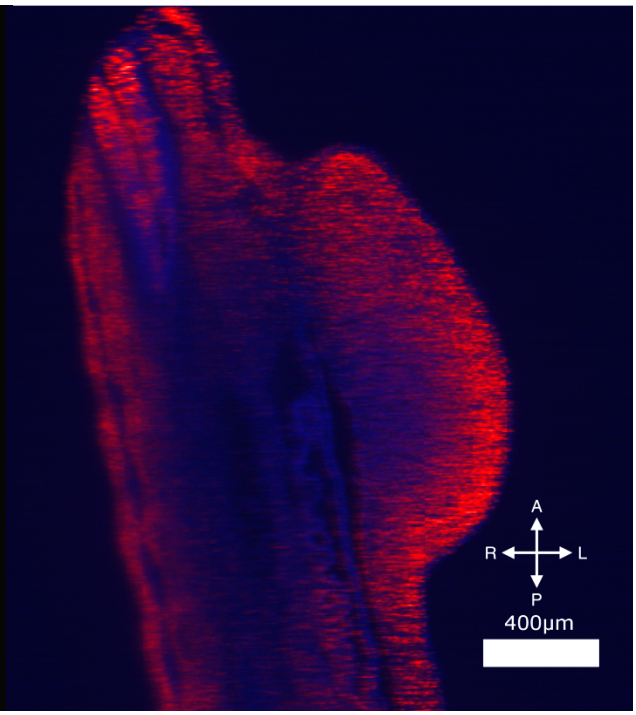

Figure 21 *Virtual dorsal plane through the body and left forelimb of a chick embryo at stage HH20. Apart from the limb at the right side of the image, parts of the spine and somites are visible. Red dots represent cells that have incorporated EdU during synthesis and have been stained with Cy3. Blue dots show the cell nuclei that were stained with DAPI.*
A: anterior, P: posterior, R: right, L: left

Hindlimbs

Cell proliferation looks quite uniform in the whole limb (Figure 22Figure 23). There seem to be fewer cells proliferating on the proximal side of the limb though, as well as more labeled

cells near the distal outskirt of the limb (Figure 22Figure 23). Furthermore, the border around the limb can be observed here in the same manner as at stage HH18 (Figure 22).

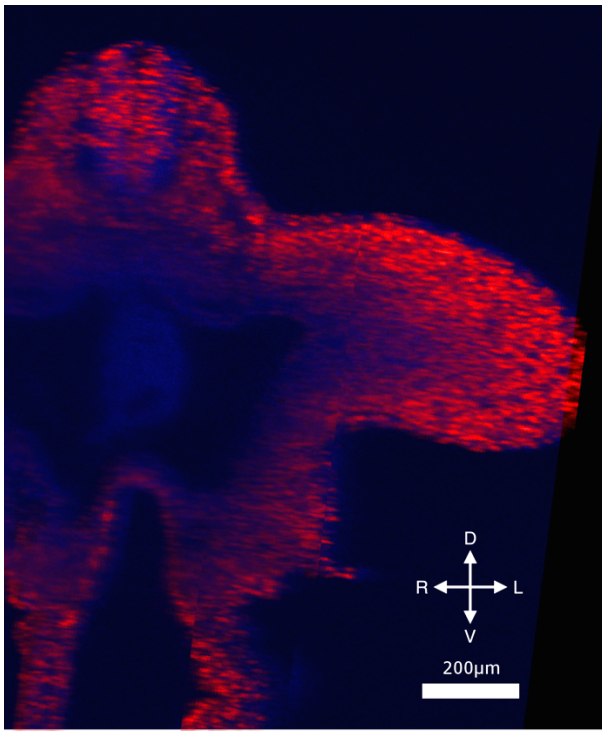

Figure 22 *Virtual cross section through the body and left hindlimb of a chick embryo at stage HH20. At the top of the image the neural tube can be seen. More cells in the limb were EdU labeled distally. Red dots represent cells that have incorporated EdU during synthesis and have been stained with Cy3. Blue dots show the cell nuclei that were stained with DAPI.*
D: dorsal, V: ventral, R: right, L: left

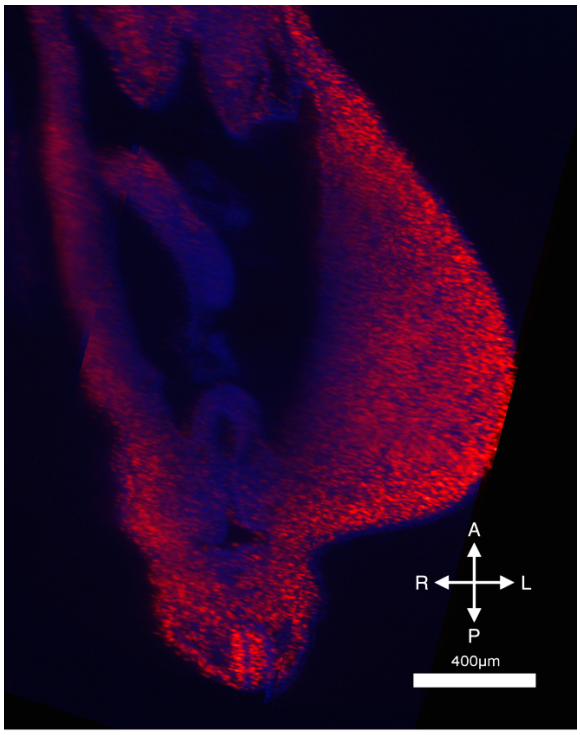

Figure 23 *Virtual dorsal section through the lower body and the left hindlimb of a chick embryo at stage HH20. At the bottom of the image the neural tube of the tail can be seen. More cells were labelled with EdU distally of the limb. Red dots represent cells that have incorporated EdU during synthesis and have been stained with Cy3. Blue dots show the cell nuclei that were stained with DAPI.*
A: anterior, P: posterior, R: right, L: left

Stage HH21

Forelimbs

Cell proliferation is uniformly distributed and occurs in the whole limb. There seems to be less cell proliferation proximally and close to the body (Figure 24). Also, there are fewer proliferating cells visible on the anterior margin (Figure 25). There is a thin layer of EdU labeled cells (couple of cells thick) around the limb (Figure 25). It is visible in the images that the aligning of the tiles after LSFM imaging was not done perfectly (noticeable as sharp edges seen in Figure 24). Still the labeled cells and their positions can be seen nicely.

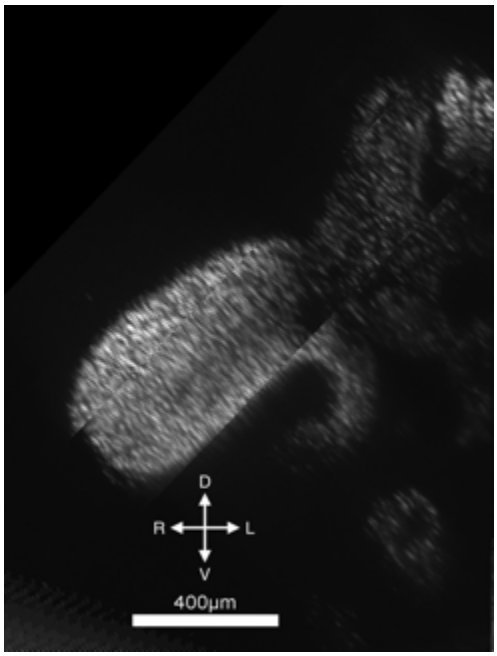

Figure 24 *Virtual cross section through the right forelimb of a chick embryo at stage HH21. In this image sharp edges can be seen due to bad alignment of the tiles after LSFM imaging. Still the overall pattern of proliferating cells can be observed. Growth seems to be uniform throughout the limb. White dots represent cells that have incorporated EdU during synthesis and have been stained with Cy3.*
D: dorsal, V: ventral, R: right, L: left

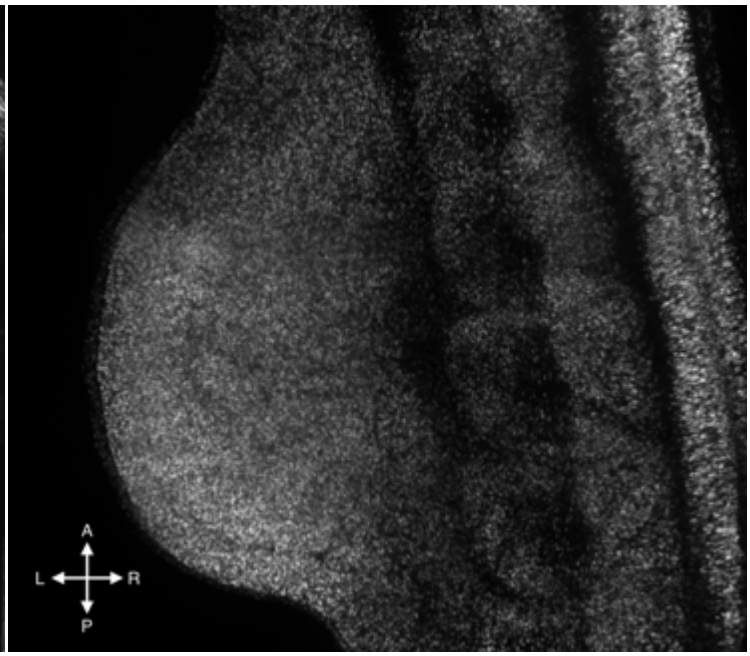

Figure 25 *Virtual dorsal section through the left forelimb of a chick embryo at stage HH21. In the right part of the image parts of the spine as well as somites can be seen. The proliferating cells in the limb show a quite uniform pattern. White dots represent cells that have incorporated EdU during synthesis and have been stained with Cy3.*
A: anterior, P: posterior, L: left, R: right

Hindlimbs

Growth looks quite uniform, but with less proliferation closer to the body of the embryo (**Figure 26Figure 27**). Both proximal in the limb, as well as in the center of the limb less EdU labeled cells can be observed. As the DAPI stain is uniform throughout the whole limb, this lack is due to less cell proliferation and not a lack of cell nuclei in general. The just a few cells thick layer around the limb is still visible at this stage, but less obvious than in earlier developmental stages (**Figure 27**). There seems to be more proliferating cells at the posterior margin, as well as dorsally (**Figure 26Figure 27**). Here as well an insufficient alignment of tiles after LSFM is visible as sharp edges in the images (Figure 26Figure 27).

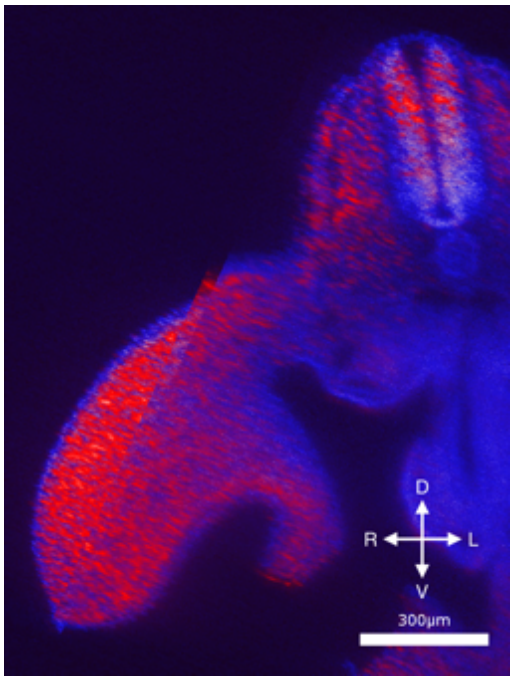

Figure 26 *Virtual cross section of a chick embryo at stage HH21 at the level of the hindlimbs. In the top part of the image the spine is visible. The limb shows proliferating cells throughout the limb, but in higher density distally. A sharp edge is visible in this image, which results from inexact alignment of the images acquired from the LSFM. Red dots represent cells that have incorporated EdU during synthesis and have been stained with Cy3. Blue dots show the cell nuclei that were stained with DAPI.*
D: dorsal, V: ventral, R: right, L: left

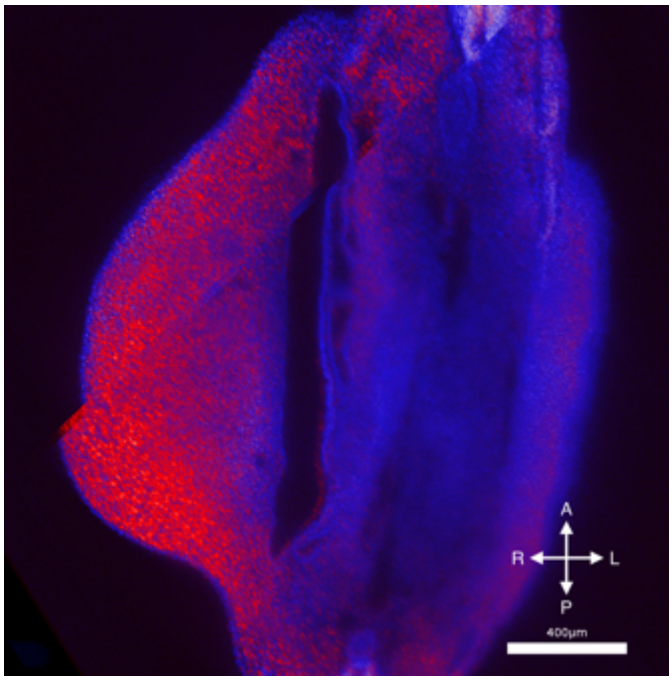

Figure 27 *Virtual dorsal section through the right hindlimb of a chick embryo at stage HH21 visible in the left part of the image. Due to imperfect alignment of the images taken with the LSFM a sharp edge is visible in the image, but does not eliminate the possibility to make statements about the cell proliferation pattern. Proliferating cells can be seen throughout the limb with a higher density distally. Red dots represent cells that have incorporated EdU during synthesis and have been stained with Cy3. Blue dots show the cell nuclei that were stained with DAPI.*
A: anterior, P: posterior, R: right, L: left

Stage HH25-

Forelimbs

There is less or even a lack of cell proliferation in the center of the forelimb, which in the cross section is seen as a circle shaped area (Figure 29). The distal third of the limbs shows overall more cell proliferation than the other two thirds (Figure 28). The center shows hardly any cell proliferation (Figure 28Figure 29). DAPI staining was not strong in this sample, which resulted in a low contrast scan, but the pattern looks uniform nonetheless (Figure 28Figure 29).

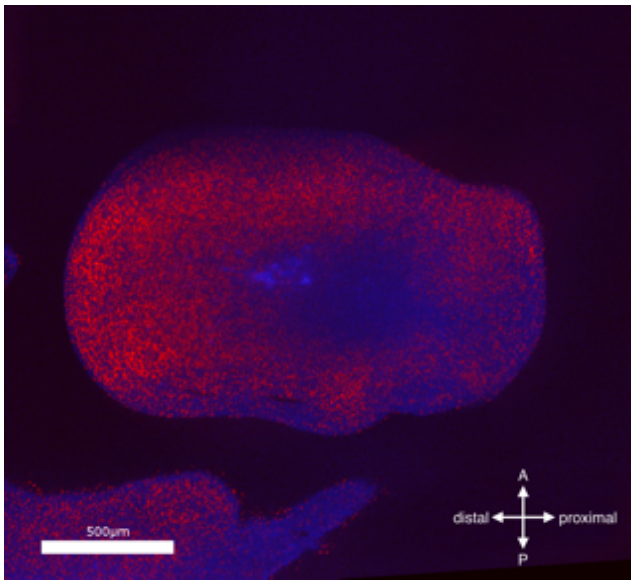

Figure 28 *Virtual section through the left forelimb of a chick embryo at stage HH25-. Just a few to almost no proliferating cells are visible in the center of the limb. There also seems to be more cell proliferation happening distally. Red dots represent cells that have incorporated EdU during synthesis and have been stained with Cy3. Blue dots show the cell nuclei that were stained with DAPI.*
A: anterior, P: posterior

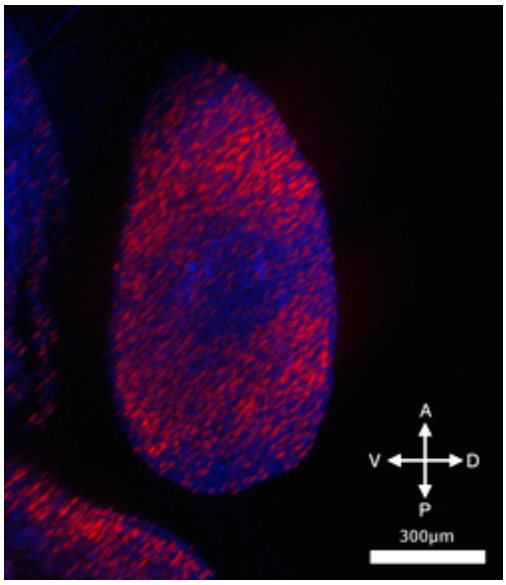

Figure 29 *Virtual section through the left forelimb of a chick embryo at stage HH25-. There are less cells proliferating in the center of the limb, compared to the areas closer to the surface. Red dots represent cells that have incorporated EdU during synthesis and have been stained with Cy3. Blue dots show the cell nuclei that were stained with DAPI. A: anterior, P: posterior, V: ventral, D: dorsal*

Hindlimbs

On the distal part of the limb the amount of cell proliferation seems to be higher than in the rest of the limb. The center area shows no or only small signs of cells proliferating (Figure 30Figure 32). Cells on the ventral side of the limb close to the body seem to show less proliferation compared to the dorsal side close to the body (Figure 32). Furthermore, the area in the middle of the limb shows less EdU labeled cells than the distal and also very proximal part of the limb (Figure 31). The distal widening of the limb is visible at this stage.

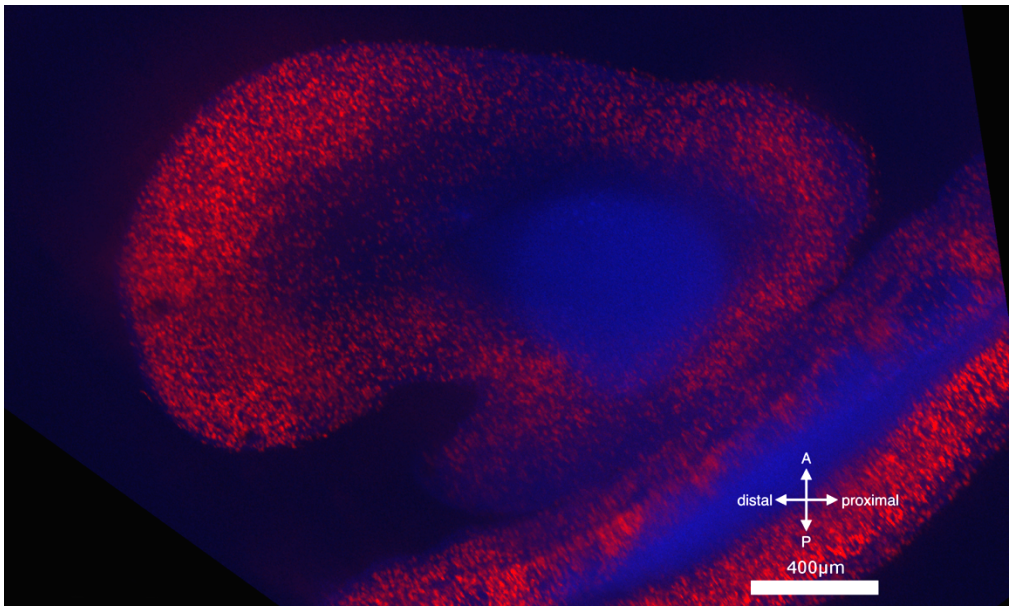

Figure 30 *Virtual section through the left hindlimb of a chick embryo at stage HH25-. In the center of the limb almost no proliferating cells can be observed. Distally there are more cells that have EdU incorporated. Red dots represent cells that have incorporated EdU during synthesis and have been stained with Cy3. Blue dots show the cell nuclei that were stained with DAPI. A: anterior, P: posterior*

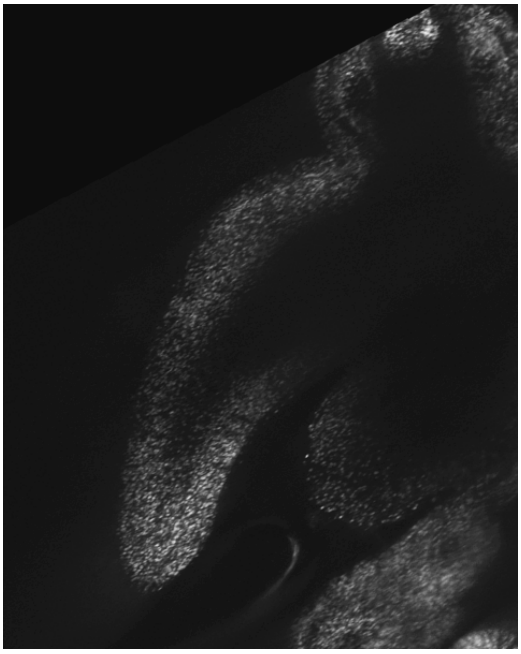

Figure 31 *Virtual section through the left hindlimb of a chick embryo at stage HH25-. The limb is visible in the left part of the image; at the top right corner a part of the spine is visible. The density of proliferating cells seems to be higher distally. There are no to very few cells that have incorporated EdU visible in the center of the limb. White dots represent cells that have incorporated EdU during synthesis and have been stained with Cy3.*

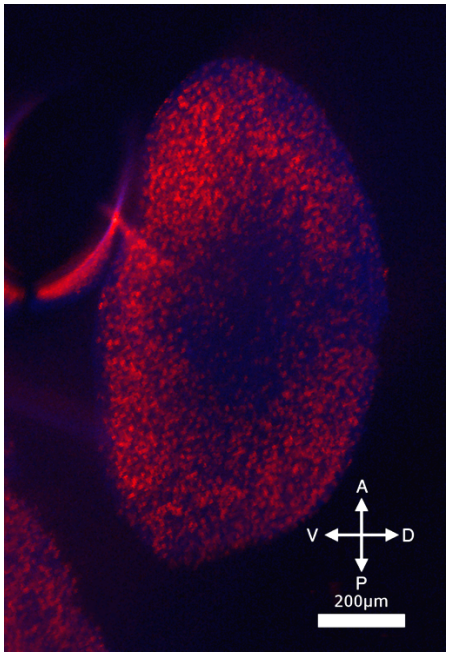

Figure 32 *Virtual section through the left hindlimb of a chick embryo at stage HH25-. The ventral side of the limbs shows more cells proliferating than the dorsal side. Red dots represent cells that have incorporated EdU during synthesis and have been stained with Cy3. Blue dots show the cell nuclei that were stained with DAPI.*
A: anterior, P: posterior, V: ventral, D: dorsal

Stage HH25

Forelimbs

No cells were labeled with EdU or DAPI in the center of the forelimb (Figure 33). There is a thicker area of cell proliferation on the dorsal side compared to the ventral side of the limb (Figure 34). It seems as if there is a bit more proliferation at the distal part compared to the more proximal part of the limb (Figure 33). There seems to be an area on the ventral side of the limb that has not been labeled with EdU. Based on the DAPI staining no damage to the limb is seen that could explain this lack of proliferating cells (**Figure 35** – DAPI volume rendering that shows no hole). In the 3D volume rendering of the limb, based on the DAPI staining, the AER is clearly visible on the distal outskirt of the limb (**Figure 35**). There is cell proliferation visible in the AER, but more just proximal to it (Figure 33).

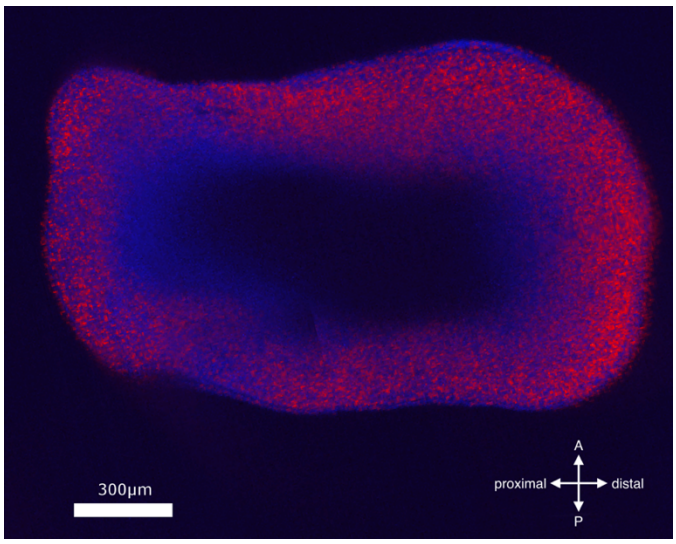

Figure 33 *Virtual section through the right forelimb of a chick embryo at stage HH25. There are only a few to no cells stained in the center of the limb. Red dots represent cells that have incorporated EdU during synthesis and have been stained with Cy3. Blue dots show the cell nuclei that were stained with DAPI. A: anterior, P: posterior*

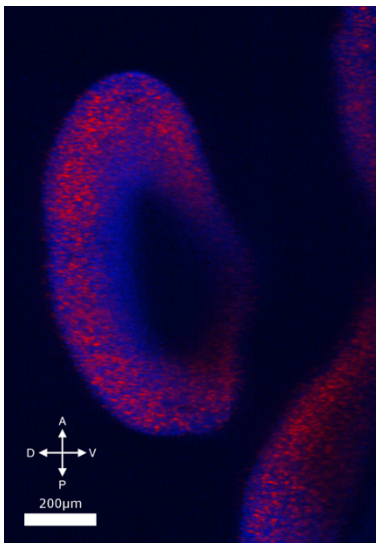

Figure 34 *Virtual section through the right hindlimb of a chick embryo at stage HH25. More cell proliferation is visible dorsally, compared to the center and ventral side of the limb. Red dots represent cells that have incorporated EdU during synthesis and have been stained with Cy3. Blue dots show the cell nuclei that were stained with DAPI.*
A: anterior, P: posterior, D: dorsal, V: ventral

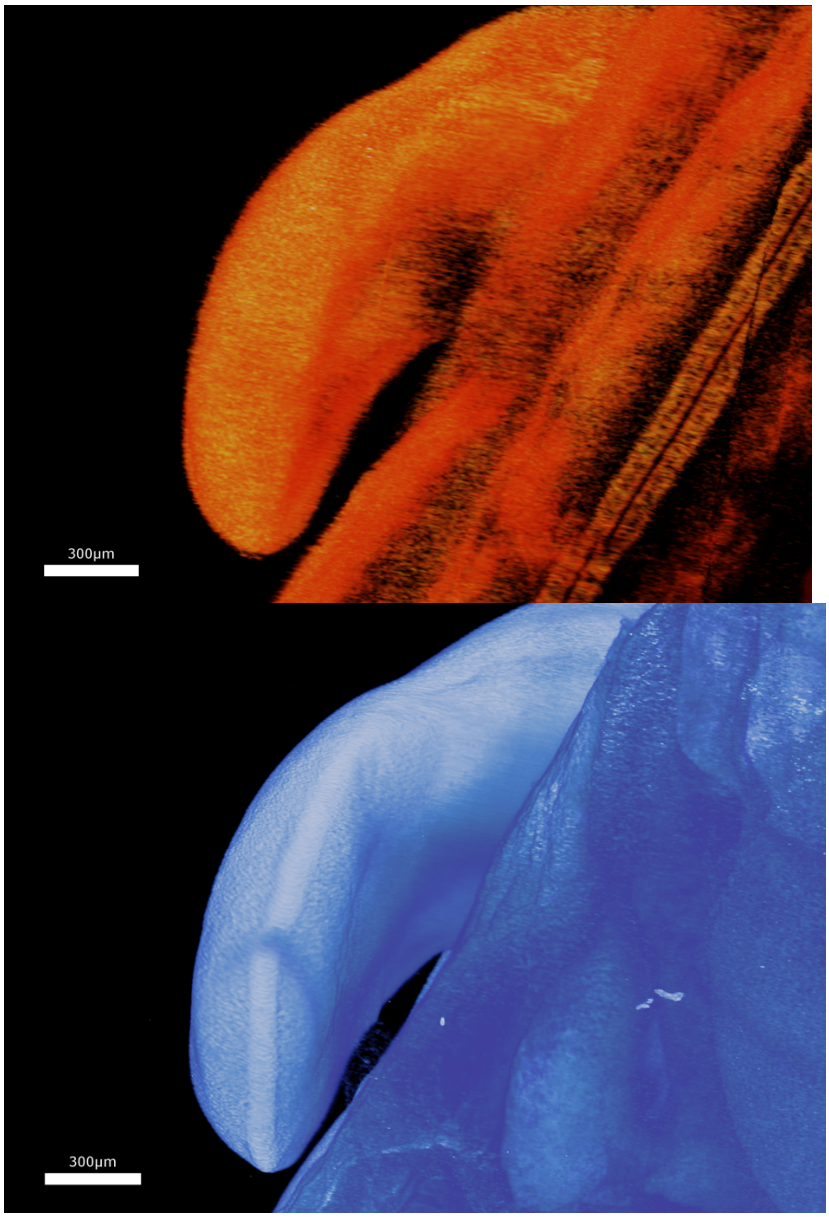

Figure 35 *3D volume renderings of the right forelimb of a stage HH25 chick embryo. Top: Rendering based on EdU labeled cells. On the ventral side of the limb an area of non-labeled cells is visible. Bottom: Rendering based on DAPI staining. In this image cells were labeled in the same area that shows a lack of proliferating cells in the top image.*

Hindlimbs

There is no cell proliferation visible in the center of the limb. There seems to be more proliferation on the distal part of the limb compared to the rest (Figure 36). Furthermore, there is a bit less cell proliferation on the ventral side of the limb compared to the dorsal side (Figure 37). The alignment of the tiles after LSFM imaging was not done perfectly, which is visible as a sharp edge in the images (Figure 36).

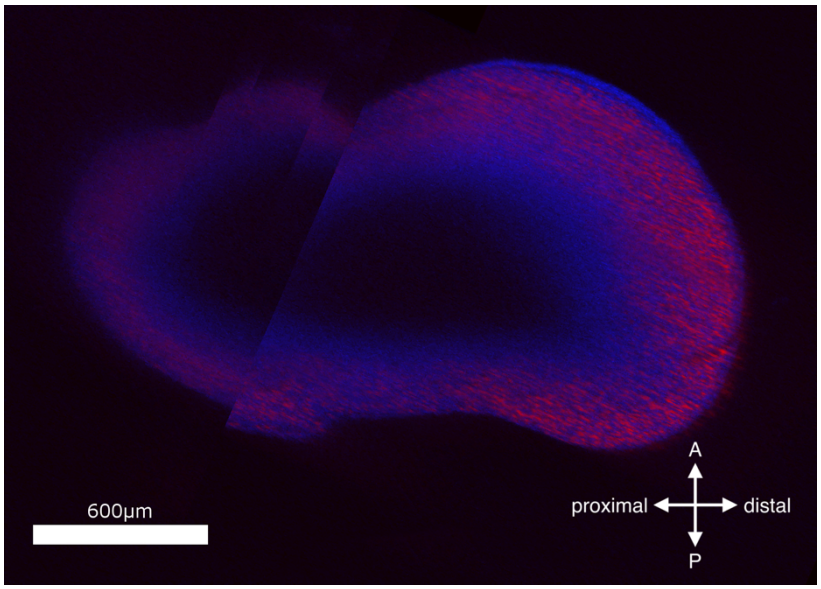

Figure 36 *Virtual section through the right hindlimb of a chick embryo at stage HH25. A sharp edge is visible in the image due to bad alignment of the images after LSFM. An area of no cell proliferation or cells labeled with DAPI is visible in the center of the limb. Red dots represent cells that have incorporated EdU during synthesis and have been stained with Cy3. Blue dots show the cell nuclei that were stained with DAPI. A: anterior, P: posterior*

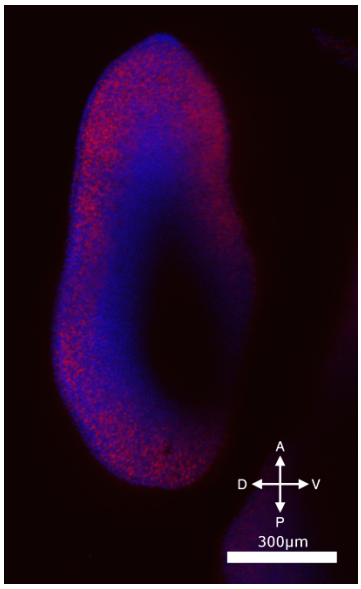

Figure 37 *Virtual section through the right hindlimb of a chick embryo at stage HH25. The ventral side and the center of the limbs shows little to no cell proliferation. Red dots represent cells that have incorporated EdU during synthesis and have been stained with Cy3. Blue dots show the cell nuclei that were stained with DAPI. A: anterior, P: posterior, D: dorsal, V: ventral*

Stage HH26-

Forelimbs

There is a lack of cell proliferation in the center of the limb, as well as a smaller area that lacks cell nuclei staining by DAPI as well (Figure 38Figure 39). The area of cell proliferation on the dorsal side of the limb is slightly thicker compared to the ventral side (Figure 38Figure 41). The bend of the elbow is already clearly visible at this stage. Areas proximal of the elbow bend show a smaller amount of EdU labeled cells (Figure 40).

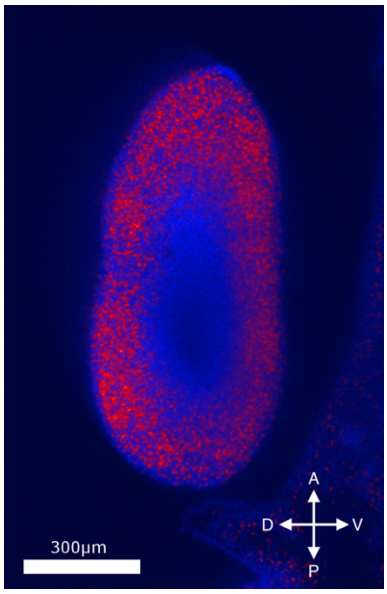

Figure 38 *Virtual section through the left forelimb of a chick embryo at stage HH26-. There is no cell proliferation visible in the center of the limb. The area on the dorsal side of the limb seems to be thicker than on the ventral side. Red dots represent cells that have incorporated EdU during synthesis and have been stained with Cy3. Blue dots show the cell nuclei that were stained with DAPI. A: anterior, P: posterior, D: dorsal, V: ventral*

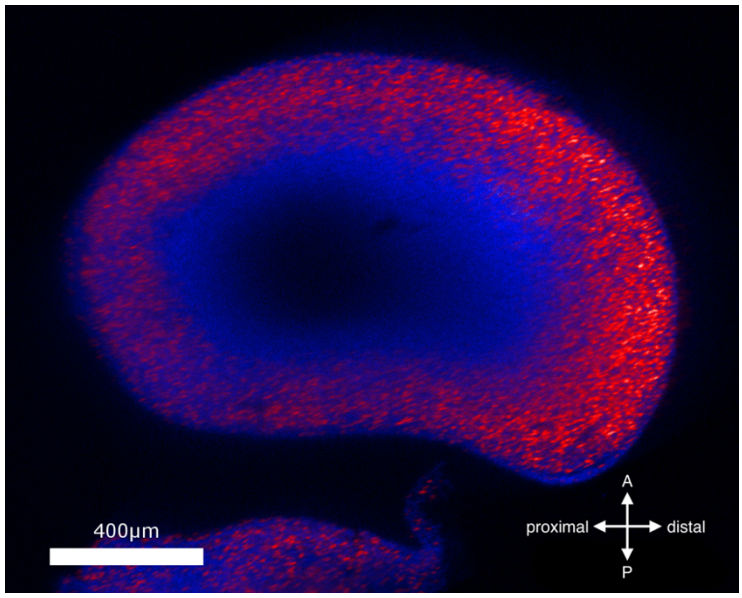

Figure 39 *Virtual section through the left forelimb of a chick embryo at stage HH26-. In the center of the limb no cell proliferation is visible. There is a higher density of proliferating cells on the distal side of the limb. Red dots represent cells that have incorporated EdU during synthesis and have been stained with Cy3. Blue dots show the cell nuclei that were stained with DAPI. A: anterior, P: posterior*

Hindlimbs

The LSFM scans of the hindlimbs at this stage were too bad in quality to be included in the analysis. The alignment was quite bad, but would have still allowed for describing the pattern if taken into account. Unfortunately, the sample seemed to have moved during the scan, or was not perfectly in focus which led to quite blurry images (Figure 42). This was the main reason for excluding this sample from the analysis.

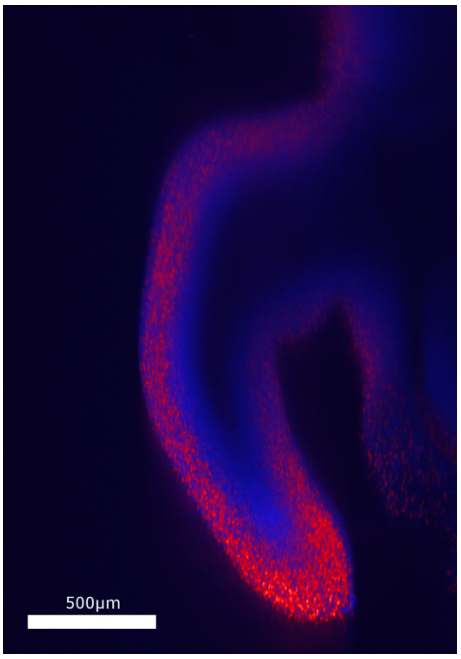

Figure 40 *Virtual cross section through the left forelimb of a chick embryo at stage HH26-. There is no cell proliferation visible in the center of the limb. Red dots represent cells that have incorporated EdU during synthesis and have been stained with Cy3. Blue dots show the cell nuclei that were stained with DAPI.*

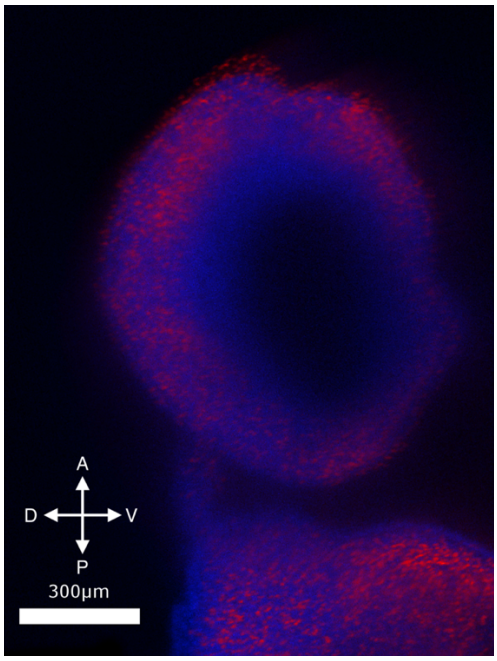

Figure 41 *Virtual section through the left forelimb of a chick embryo at stage HH26-. The center of the limb shows no cell proliferation. Also the density of proliferating cells closer to the surface is rather low. Red dots represent cells that have incorporated EdU during synthesis and have been stained with Cy3. Blue dots show the cell nuclei that were stained with DAPI.*
A: anterior, P: posterior, D: dorsal, V: ventral

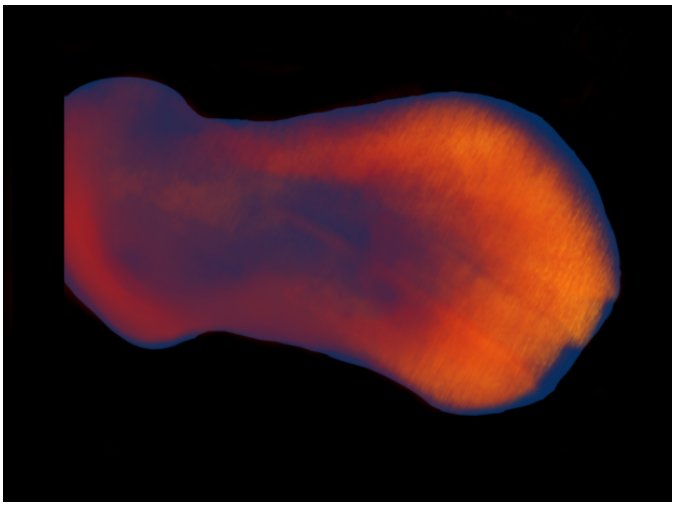

Figure 42 *3D volume rendering of the hindlimb of a chick embryo at stage HH26-. It is clearly visible that the alignment of pictures after LSFM is quite bad. The individual cells are also quite blurry and therefore limit the possibilities of describing cell proliferation patterns in this limb. Therefore, this sample was excluded from the analysis.*

Stage HH27-

Forelimbs

The quality of the scan of the forelimbs at this stage was unfortunately too poor to be used for analysis.

Hindlimbs

The distal part of the limb is wider and flatter than the rest at this developmental stage (Figure 43). Within the distal part (foot) are three areas of less cell growth, which corresponds to the developing digits (Figure 43 andFigure **44**). In the leg the center does only show very little to no cell proliferation (Figure 45Figure 46). There seems to be another area of little to no EdU labeled cells between the part within the leg and the three areas in the foot (Figure 43 and Figure **44**). Near the surface there seems to be more proliferating cells anterior and posterior than in the midline, throughout the limb (Figure 44Figure 45). More labeled cells are visible distally compared to proximally (Figure 43).

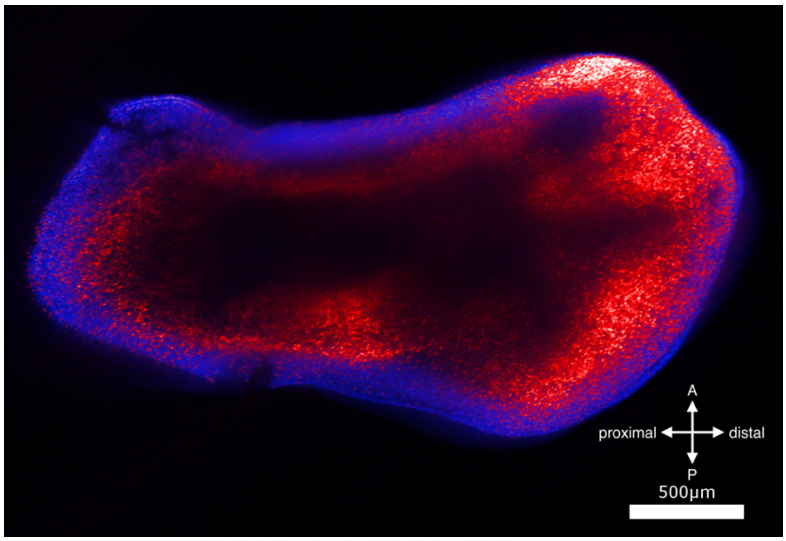

Figure 43 *Virtual section through the right hindlimb of a chick embryo at stage HH27-. Little to no proliferating cells can be observed in the center of the limb as well as in parts of the foot paddle. Red dots represent cells that have incorporated EdU during synthesis and have been stained with Cy3. Blue dots show the cell nuclei that were stained with DAPI. A: anterior, P: posterior*

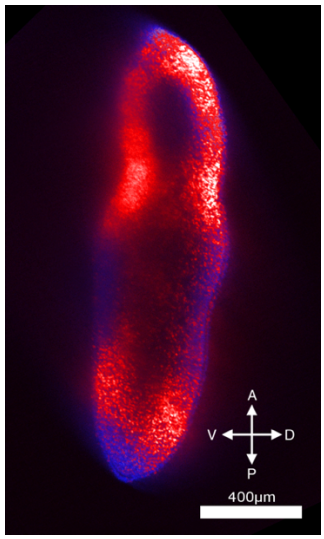

Figure 44 *Virtual cross section through the right foot paddle of a chick embryo at stage HH27-. Different densities of cell proliferation can be observed with the biggest lack in the center of the paddle.*

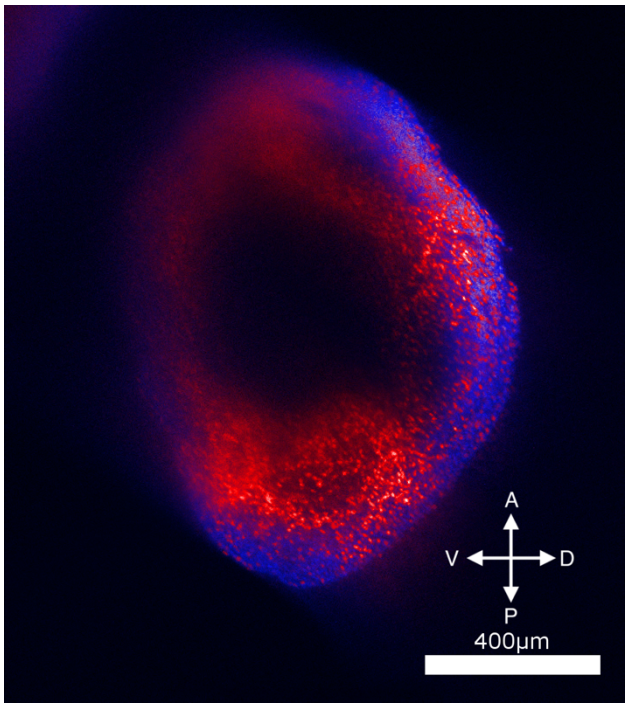

Figure 45 *Virtual section through the right leg of a chick embryo at stage HH27-. The center of the limb shows no proliferating cells. Red dots represent cells that have incorporated EdU during synthesis and have been stained with Cy3. Blue dots show the cell nuclei that were stained with DAPI. A: anterior, P: posterior, D: dorsal, V: ventral*

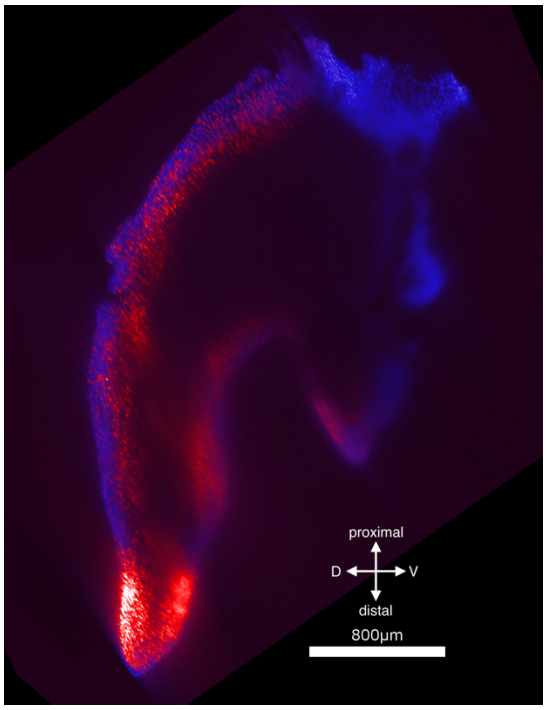

Figure 46 *Virtual section through the right hindlimb of a chick embryo at stage HH27-. Areas towards the body show little to no cell proliferation. The density of cells that have incorporated EdU is highest at the tip of the limb. Red dots represent cells that have incorporated EdU during synthesis and have been stained with Cy3. Blue dots show the cell nuclei that were stained with DAPI. D: dorsal, V: ventral*

Stage HH28

Forelimbs

The quality of the scan of the forelimbs at this stage was unfortunately too poor to be used for analysis. The sample was probably damaged while mounting, as it is hardly possible to identify the limb and other parts of the sample from the obtained images (Figure 47).

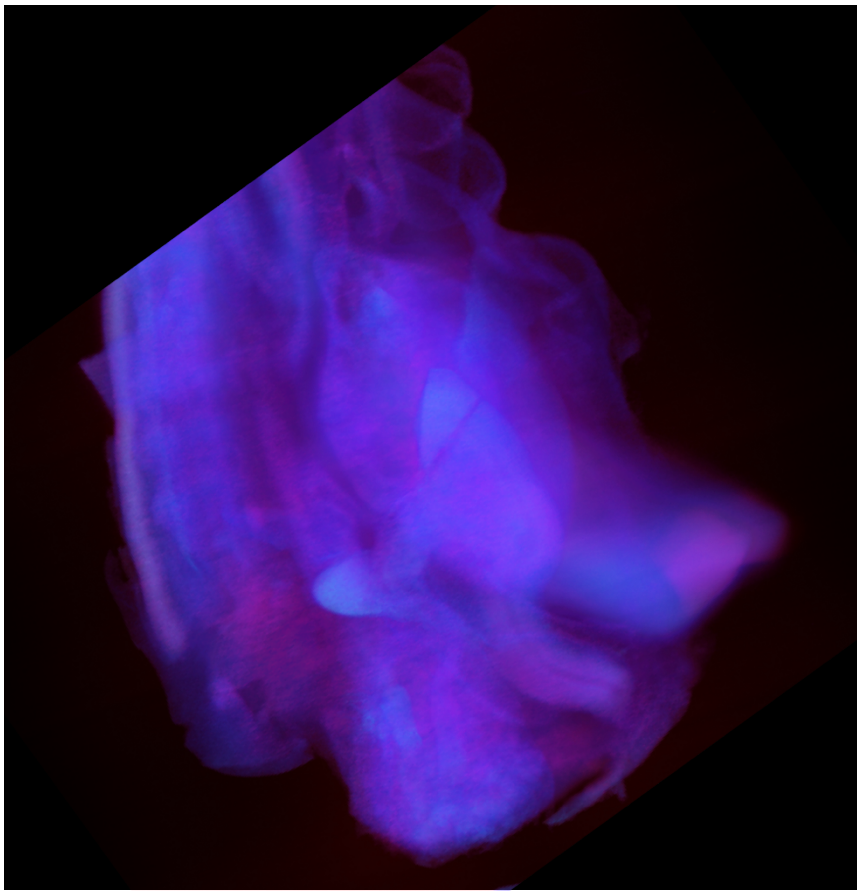

Figure 47 *3D volume rendering of a chick embryo at stage HH28, at the level of the forelimbs. The sample looks quite damaged and it is not possible to get information about cell proliferation patterns from this image stack. Red areas represent cells that have incorporated EdU during synthesis and have been stained with Cy3. Blue areas show the cell nuclei that were stained with DAPI.*

Hindlimbs

In the distal and wider part of the limb, the foot paddle, three areas of no or little cell growth can be observed (Figure 48). The cross section shows that these areas are somewhat circular shaped and have dorsoventral dents between them (Figure 49). This corresponds well with the position of the forming digits. Furthermore, in the center of the circular shapes cell proliferation is visible, which results in a more ring shaped area of only a few to no EdU labeled cells.

In the leg two long tube-shaped areas show a bigger amount of cell proliferation compared to other areas in the arm (Figure 48Figure 50). Between these two areas there are less EdU labeled cells (Figure 48 and 50). The distal part of the foot as well as the distal part of the leg near it, have more cells labeled compared to the proximal part of both (Figure 48Figure 50).

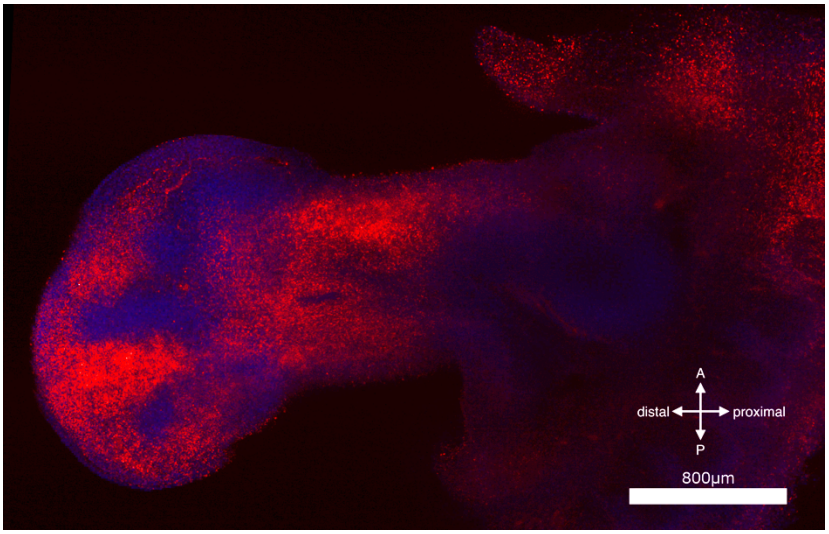

Figure 48 *Virtual section through the left hindlimb of a chick embryo at stage HH28. The well defined foot paddle shows separate areas of very little cell proliferation. Also the leg shows areas of little cell proliferation in the center and more uniform and denser areas around it. Red dots represent cells that have incorporated EdU during synthesis and have been stained with Cy3. Blue dots show the cell nuclei that were stained with DAPI.*
A: anterior, P: posterior

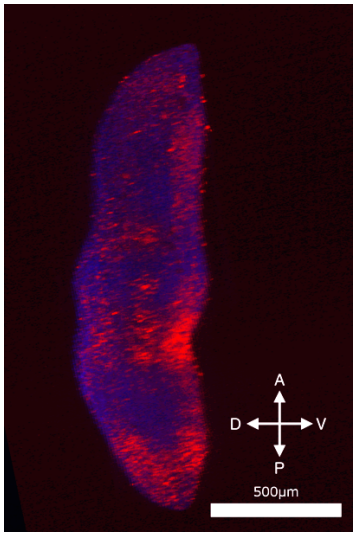

Figure 49 *Virtual section through the left foot paddle of a chick embryo at stage HH28. Forming digits can be seen as areas of few proliferating cells along the center plane of the paddle. Red dots represent cells that have incorporated EdU during synthesis and have been stained with Cy3. Blue dots show the cell nuclei that were stained with DAPI.*
A: anterior, P: posterior,
D: dorsal, V: ventral

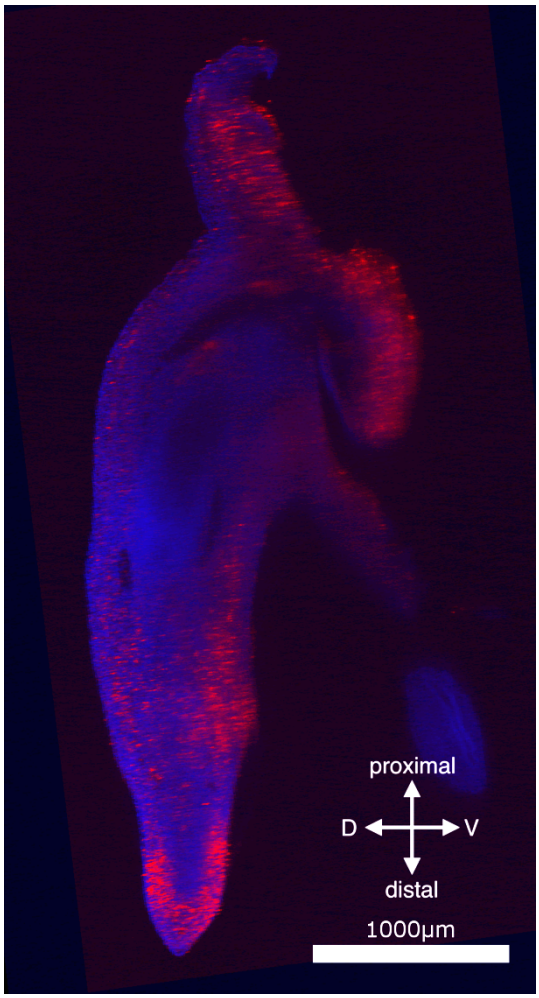

Figure 50 *Virtual section through the left hindlimb of a chick embryo at stage HH28. In the middle of the leg cells are proliferating less than in areas closer to the surface. At the tip of the foot – seen in the bottom of the image – a presumed forming digit can be seen as a zone of very little cell proliferation. Red dots represent cells that have incorporated EdU during synthesis and have been stained with Cy3. Blue dots show the cell nuclei that were stained with DAPI. D: dorsal, V: ventral*

Stage HH31

Forelimbs

The distal part of the limb is wider and flatter than the rest and by that the autopod can be distinguished from the arm. Within the autopod, areas of high as well as little to no cell proliferation can be observed (Figure 51). These areas resemble presumably the forming skeletal elements of the digits (low cell proliferation), as well as the areas close to the future joints (high cell proliferation). Proximal to the assumed digits another area of only a few EdU labeled cells can be observed, which corresponds well with the position of the developing metacarpus and carpus (Figure 51).

As the elbow is visible, the arm can now be clearly distinguished into zeugopod and stylopod. In the first two tube-like areas of little to no cell proliferation, as well as no cell nuclei stain by DAPI, can be seen (Figure 51Figure 52Figure 53). The stylopod shows mostly no or only little cell proliferation, which might have resulted from insufficient staining (Figure 53). With the help of the DAPI staining the outline of the femur can be seen, as well as the outlines of both the ulna and radius (Figure 51Figure 53). Also cell proliferation is partly happening in the areas of the forming ulna and radius (Figure 51Figure 53).

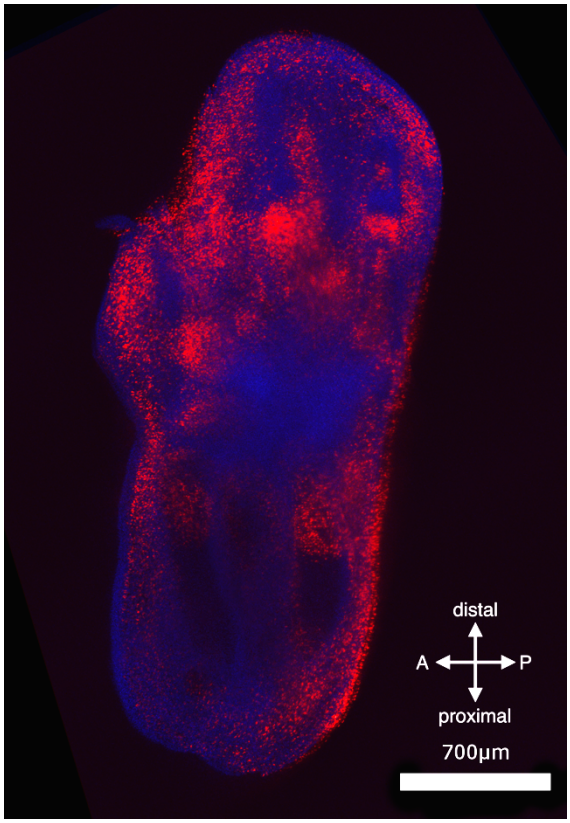

Figure 51 *Virtual section through right forelimb of a chick embryo at stage HH31. In the hand paddle areas of little to no cell proliferation are visible. These areas correspond well to the position of forming phalanges, metacarpus and carpus. In the zeugopod the areas of little to no cell proliferation correspond well to the position of the forming radius and ulna. Red dots represent cells that have incorporated EdU during synthesis and have been stained with Cy3. Blue dots show the cell nuclei that were stained with DAPI. A: anterior, P: posterior*

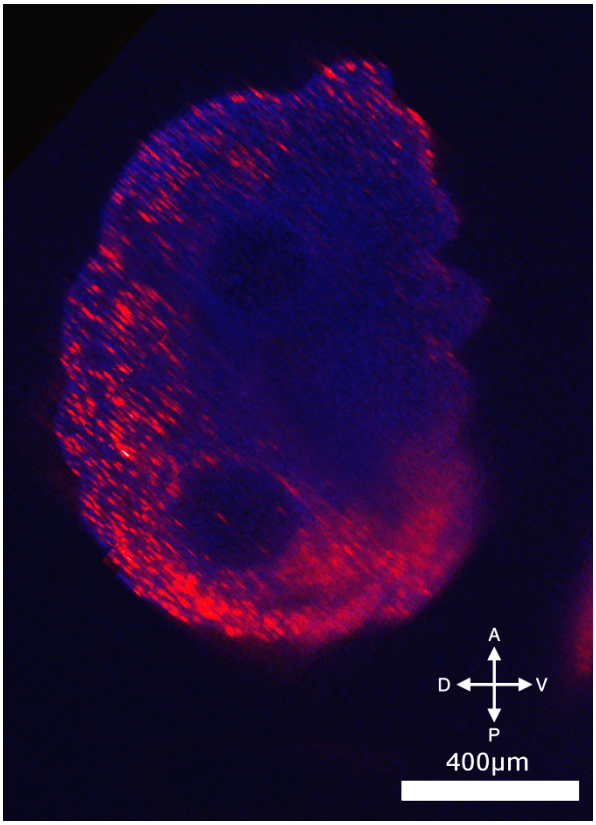

Figure 52 *Virtual cross section through the right zeugopod of a chick embryo at stage HH31. Two circular areas in the center of the limb show almost no cell proliferation nor stained cell nuclei. These two areas correspond well to the position of the forming radius and ulna. Red dots represent cells that have incorporated EdU during synthesis and have been stained with Cy3. Blue dots show the cell nuclei that were stained with DAPI.*
A: anterior, P: posterior, D: dorsal, V: ventral

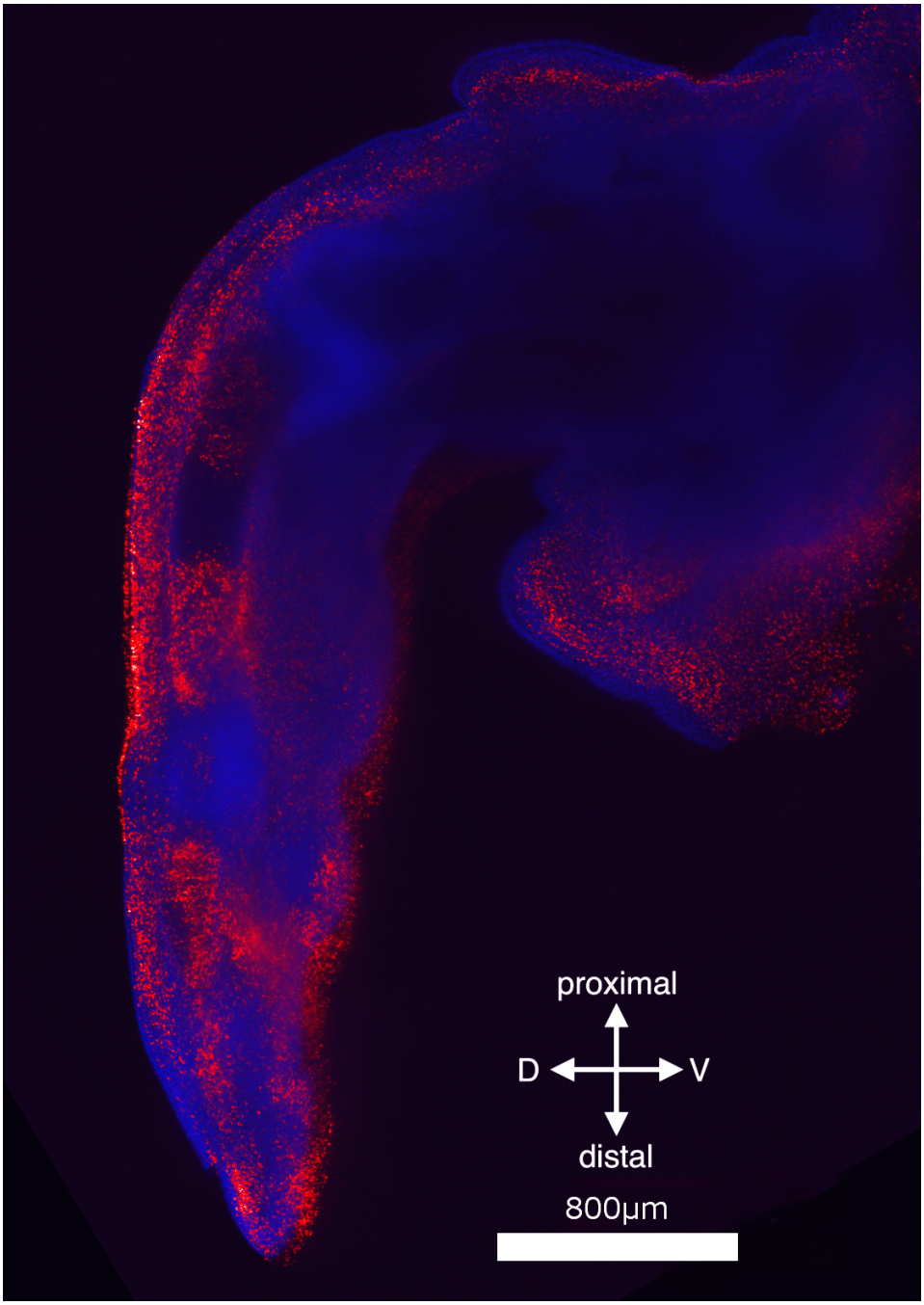

Figure 53 *Virtual section through the right forelimb of a chick embryo at stage HH31. Areas of no to little cell proliferation, as well as no stained cell nuclei in general correspond well to the forming bones in the limb. Red dots represent cells that have incorporated EdU during synthesis and have been stained with Cy3. Blue dots show the cell nuclei that were stained with DAPI. D: dorsal, V: ventral*

Hindlimbs

The forming digits are now clearly visible within the autopod from both the DAPI staining and EdU labeling (Figure 55). More cell proliferation is visible at the base of the bones forming the digits and in the areas where the future joints will be, compared to the rest of the area along the future bones which shows almost no EdU labeled cells (Figure 54). This also includes the tips of the toe bones, where no cell proliferation is seen (Figure 55). Furthermore, dorsoventral dents are visible in between the forming digits (Figure 56).
The zeugopod and stylopod can be distinguished based on the visible knee bend, as well as the outlines of the forming skeletal elements identifiable due to the DAPI staining (Figure 59). At the distal end of the limb many EdU labeled cells are visible, and at the mid-section through the foot they correspond well to the position of the AER (Figure 55, left). The spaces between the forming bones in the foot show only a few proliferating cells close to the midsection (Figure 55, left), but more labeled cells further away (Figure 54Figure 55, right).

There is an area of less proliferation proximal to the forming digits, which corresponds well to the forming metatarsus and tarsus (Figure 58). In the leg, the outline of the epiphysis of the tibia can be seen as an area of higher cell proliferation (Figure 58). The proximal part of the leg shows less to no cell proliferation in the center, which might have resulted from insufficient penetration from the EdU (Figure 54). The DAPI stain shows the outlines of the forming tibia and fibula, as well as of the humerus proximal to the knee (Figure 59). In the cross section through the zeugopod two circular shapes of little to no cell proliferation is visible, as well as a spot in between these two that also shows less proliferation than the surrounding area (Figure 57).

There is one edge visible in the foot paddle which resulted from bad alignment of the tiles after the LSFM (Figure 55Figure 56). This error in alignment did not hinder the description of the pattern of proliferating cells, though.

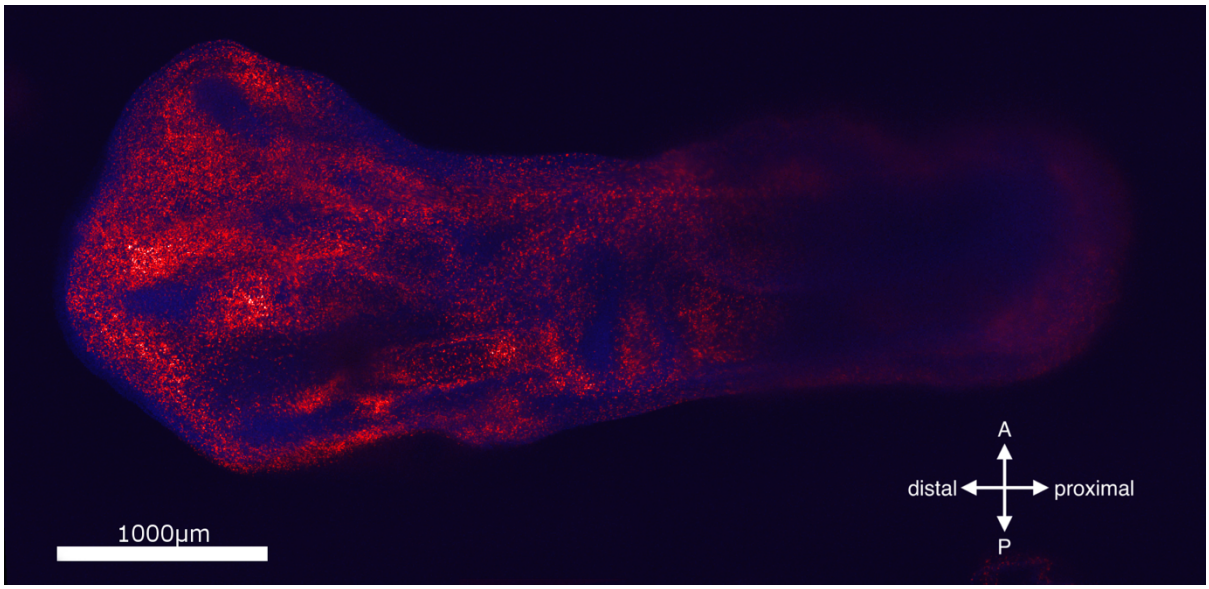

Figure 54 *Virtual section through the left hindlimb of a chick embryo at stage HH31. In the foot paddle small areas of no cell proliferation that correspond well to the forming phalanges can be seen. Proximal to the foot paddle and in the zeugopod the edges of the forming radius, ulna as well as some of the metatarsal and tarsal bones are visible. Red dots represent cells that have incorporated EdU during synthesis and have been stained with Cy3. Blue dots show the cell nuclei that were stained with DAPI. A: anterior, P: posterior*

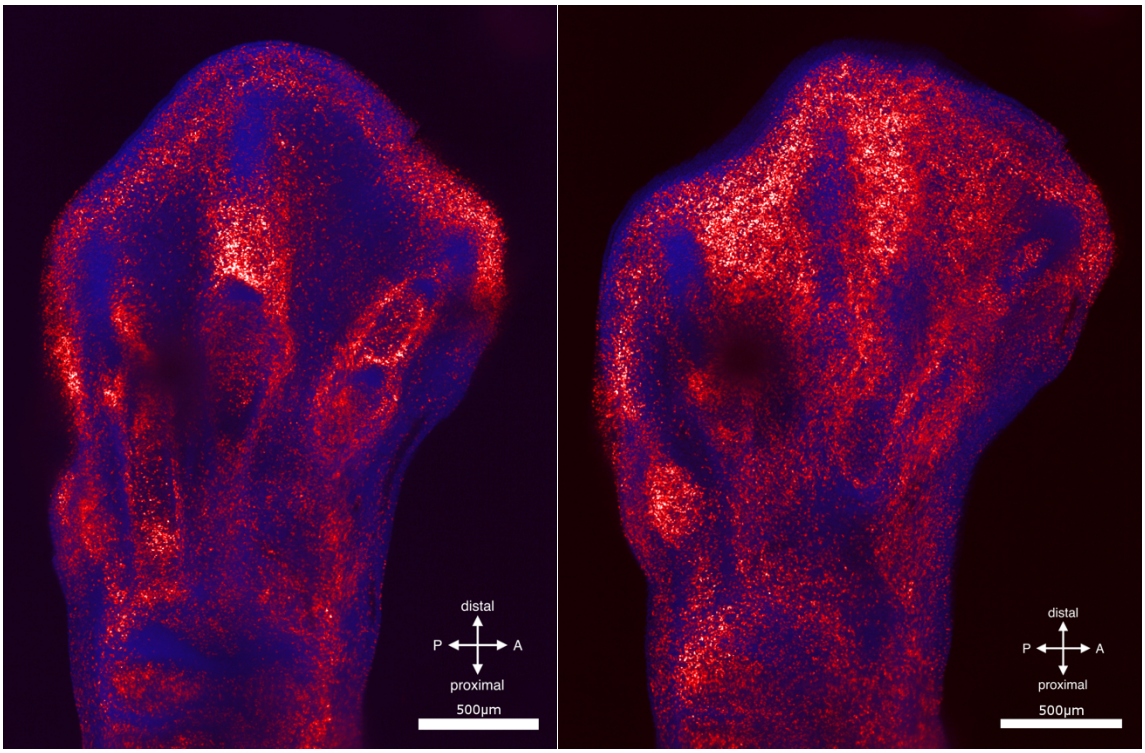

Figure 55 *Virtual sections through the left foot paddle and zeugopod of a chick embryo at stage HH31. Both sections show that the amount of proliferating cells varies around the forming phalanges, seen as areas of little to no cell proliferation interrupted by areas of many EdU incorporated cells. The right section is closer to the ventral side of the embryo compared to the left image, which is close to the middle. Red dots represent cells that have incorporated EdU during synthesis and have been stained with Cy3. Blue dots show the cell nuclei that were stained with DAPI. P: posterior, A: anterior*

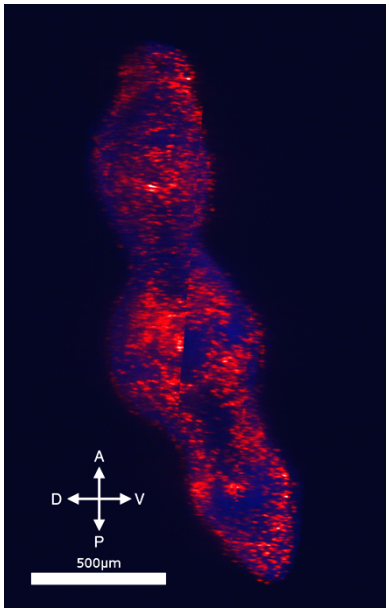

Figure 56 *Cross section through the left foot paddle of a chick embryo at stage HH31. The edge in the middle of the image resulted from bad alignment of the images after LSFM. Dents towards the center are visible as well as areas of little to no cell proliferation in the center of the limb. These areas correspond well to forming phalanges. Red dots represent cells that have incorporated EdU during synthesis and have been stained with Cy3. Blue dots show the cell nuclei that were stained with DAPI. A: anterior, P: posterior, D: dorsal, V: ventral*

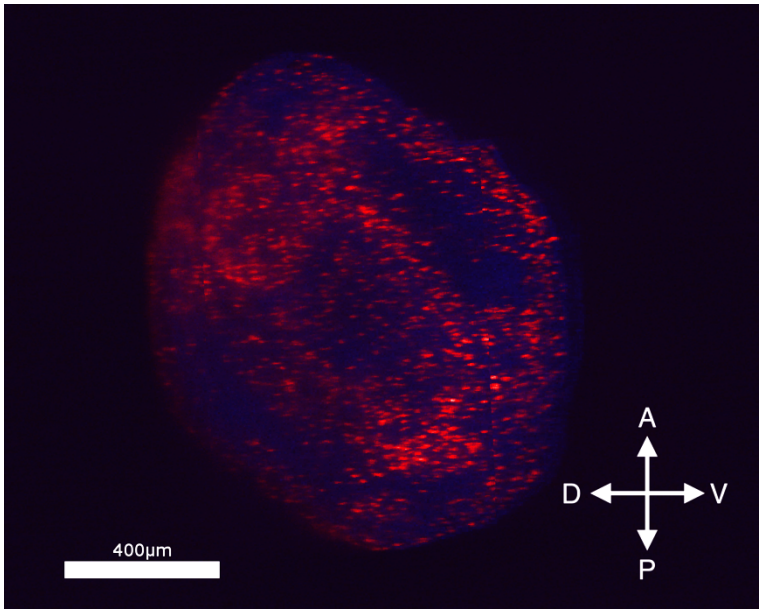

Figure 57 *Virtual section through the left zeugopod of a chick embryo at stage HH31. Areas of little to no cell proliferation in the center of the limb correspond well to the forming tibia and fibula. Red dots represent cells that have incorporated EdU during synthesis and have been stained with Cy3. Blue dots show the cell nuclei that were stained with DAPI.*
A: anterior, P: posterior, D: dorsal, V: ventral

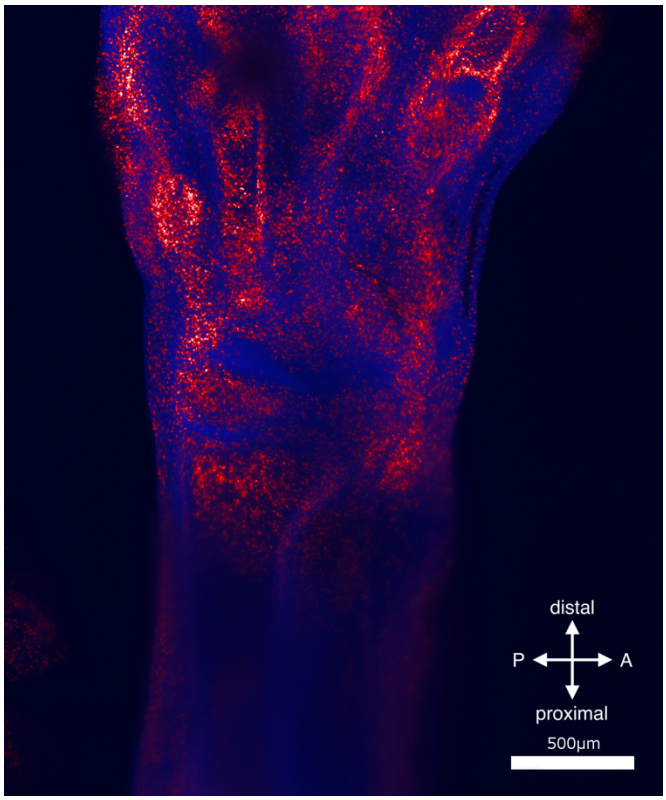

Figure 58 *Virtual section through the left hindlimb of a chick embryo at stage HH31. In focus here the area of forming tarsal and metatarsal bones. Also the epiphysis of the tibia can be seen as a zone of higher cell proliferation compared to its surrounding Furthermore, the lack of stained cell nuclei in the lower leg represent the forming tibia and fibula. Red dots represent cells that have incorporated EdU during synthesis and have been stained with Cy3. Blue dots show the cell nuclei that were stained with DAPI. P: posterior, A: anterior*

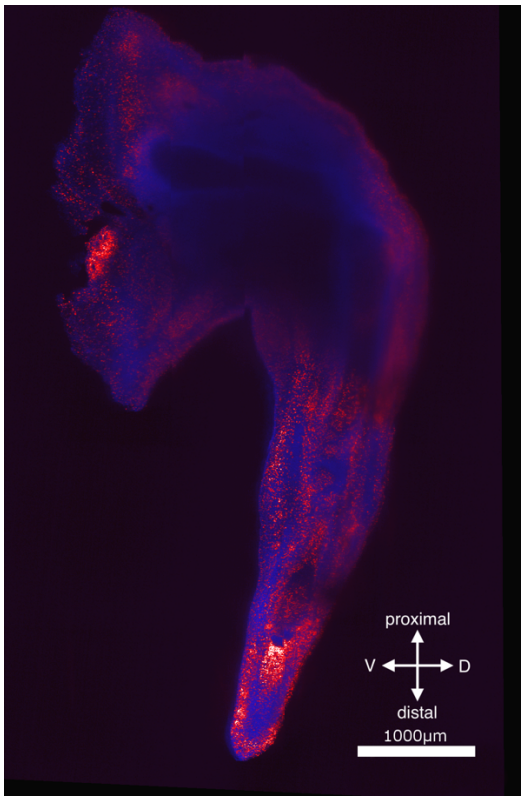

Figure 59 *Virtual section through the left hindlimb of a chick embryo at stage HH31. The forming bones in the leg can be seen as areas of no stained cell nuclei. Red dots represent cells that have incorporated EdU during synthesis and have been stained with Cy3. Blue dots show the cell nuclei that were stained with DAPI. V: ventral, D: dorsal*

Data for possible further analyses

Individual cell counts

Due to their single-cell-resolution it is possible with the acquired data to count individual cells. A test run was done on a part of the image stack of the hindlimb at stage HH31 by using the ImageJ Plugin '3D Object Counter' (Bolte & Cordelières, 2006). The resulting information showed that the centroid of single cell nuclei can be detected and localized (Figure 60). A more sophisticated method would be needed to actually count all cells in the limb, probably requiring a transformation of the stack into binary images first. This can be done as the brightness of individual labeled cells does not matter: cell nuclei are either

labeled or not. The brightness might vary due to the position of the sample within the LSFM, the amount of incorporated EdU or a combination of both. Thus segmentation of the images to generate a binary mask that localizes the cell nuclei would be possible.

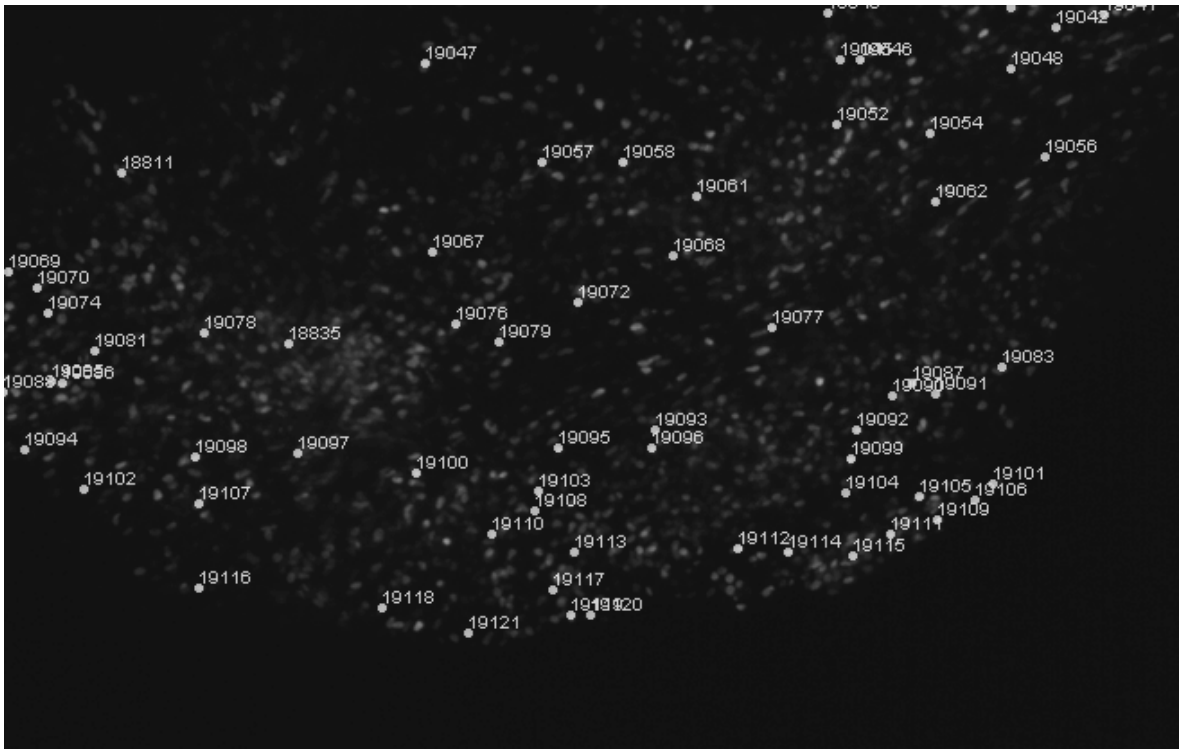

Figure 60 *Virtual section through the hindlimb of a chick embryo at stage HH31. Dots with numbers next to them refer to the cell nuclei centroids counted by the ImageJ plugin '3D Object Counter'. Gray dots represent cells that had EdU incorporated during synthesis.*

Cell density

With the data produced in this project cell density analysis can be performed. To demonstrate this, a simple and quick way to get a quantitative representation of cell density was used. All the following steps were performed using ImageJ, if not stated otherwise. First the images of the used stack were transformed into binary images, by setting a global threshold. This led to images showing EdU labeled cells in white and the background in black. As a next step the '3D Gaussian Blur' filter implemented in ImageJ was used. This resulted in different gray values in the stack, where brighter and darker areas depend on the density of the cells. Areas of cells that were close to each other would blur together to brighter areas than cells that have a bigger distance between them. As this process results in a histogram of different gray values, with bright values representing high density, a

colored transfer function can be used to overlay the data. This was done in a volume rendering in Amira.

The result shows areas of high density as yellow and low density as blue (Figure 61). In the test sample (the hindlimb at stage HH25) we can observe higher density within the limb, compared to the area close to the surface. Also differences in density between the distal and proximal areas can be seen. Here again more sophisticated procedures can be used to quantify cell densities and their changes during limb development.

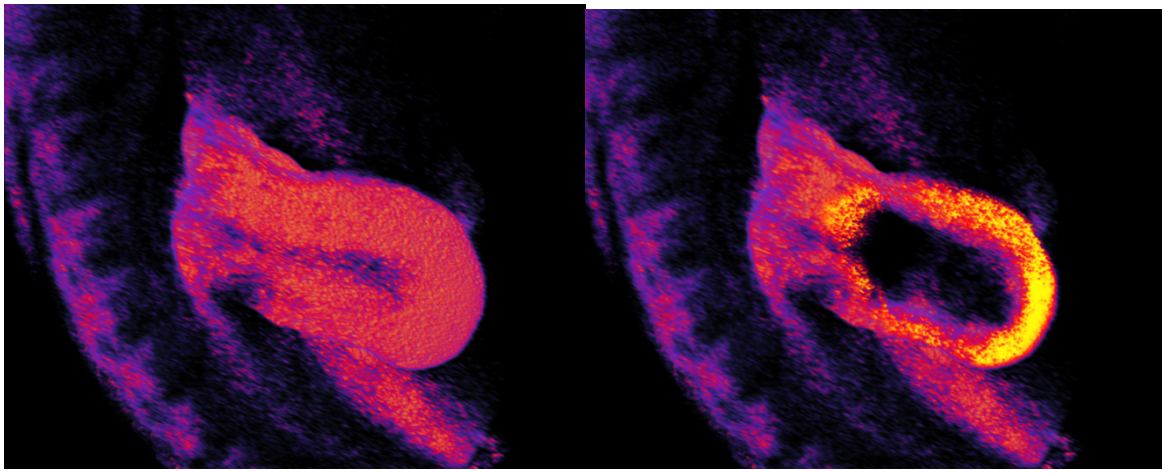

Figure 61 *3D volume renderings of a hindlimb of a chick embryo at stage HH25 showing the density of cells that had EdU incorporated during development. Left: The whole hindlimb. Right: virtual section through the middle of the hindlimb. Yellow – high proliferating cell density, blue – low proliferating cell density*

Discussion

This study has demonstrated one method for 3D imaging of cell proliferation in whole limb buds and produced a series of high-resolution volume images for developing chick limbs. This allows direct measurements of local density of proliferating cells, potentially along with simultaneous measurement of overall cell density. Fluorescent EdU chemistry was successfully used to label proliferating cells in whole chick limbs up to stage HH31. It was also shown that the labeled cells can be visualized at single-cell resolution in 3D using LFSM.

The data shown here corroborate the conclusions of the cell proliferation studies reviewed in the introduction (see page 9; Ede et al., 1975; Fernández-Terán et al., 2006; Hornbruch & Wolpert, 1970). In the imaged limbs more cell proliferation was observed distally than proximally, except for the stages HH18 and HH20 (see e.g. Figure 17Figure 23), which showed more or less uniform cell proliferation in the limb. The developing limb consists of mesenchyme that is surrounded by a layer of ectoderm. That particular layer could be observed as a layer of proliferating cells in both forelimbs and hindlimbs at the stages HH18, HH20 and HH21 (see e.g. Figure 18). In the subsequent stages the ectoderm layer was also visible, but not as clearly, and it consisted of fewer EdU labeled cells. Also the areas of precartilage condensations showed less cell proliferation (see e.g. Figure 29Figure 48). Furthermore, the patterns in the wing and leg are generally quite similar to each other during development.

At the stages HH25-, HH25 and H26- a zone of very little cell proliferation and also just a few stained cell nuclei were observed in the center of the limb. This area corresponds well with the OP, an area of cell death described in the core of the developing limb (Fell & Canti, 1934). At the stages HH25- and HH26-, the area in the center might not show sufficient staining of DAPI, which results in the dark area in the middle (see e.g. Figure 39Figure 46). The EdU labeling looks better in terms of penetration of the tissue, even though we might still miss few proliferating cells that have not been stained in the core of the limb in these two stages. At stage HH31 the regions between the zeugopod and stylopod, and the area close to the body show basically no EdU labeled cells, which is probably due to insufficient penetration of the tissue by the EdU (Figure 59). Even if there really were almost no

proliferating cells at least a few labeled cell nuclei would still be expected in these areas, which we cannot see in the image data. It has been reported that in whole embryos older than 72 hours (which would refer to a developmental stage of around HH20) EdU did not necessarily fully penetrated the tissue (Warren et al., 2009). The present data do show however, that at least the limbs, except for the areas mentioned, did show good EdU labeling even past stage HH20.

At stage HH25- there are only a few cells proliferating in the middle of the limb on the anterior margin (Figure 28Figure 30). This might correspond to the ANZ, an area of cell death described by (Saunders Jr. et al., 1962). A similar zone in terms of position was described in that study at stage HH27, which we can also see as a region of just a few proliferating cells along the anterior margin of the developing limb (Figure 43). At stage HH28 cell death in the region of the elbow is described, which might correspond to only a few labeled cells at the same stage in the data shown here (Figure 50). Cell death in this case is interpreted as a way to form the overall shape of the developing limb in chick embryos (Saunders Jr. et al., 1962).
These authors also describe the PNZ, a zone of cell death located close to the body wall and posteriorly of the limb at stage HH24 (Saunders Jr. et al., 1962). In our images at stage HH25- we see fewer proliferating cells posteriorly in the forelimb (Figure 29), but a rather uniform distribution of EdU labeled cells in the hindlimb (Figure 32). At stage HH25 cell apoptosis should still take place posteriorly, but in our data we do see cell proliferation in these areas, with maybe fewer proliferating cells in the hindlimb (Figure 33Figure 36). It was shown by Fernández-Terán and colleagues (2006) that areas of little cell proliferation correlate well with regions of cell death. So it is reasonable to assume that the areas, in which less cells were labeled with EdU, are regions where cell apoptosis is likely to occur.
At stage HH27- the hindlimb shows three, in cross section partly fused, areas of little to no proliferating cells as well as no stained cell nuclei (Figure 43Figure 43). There are two dorsoventral dents visible in the cross section through the limb, that correspond to the interdigital space. In the leg a circular shaped zone of no proliferating cells, which corresponds well to the area of forming cartilage, can be seen (Figure 45). From the images it still might be possible that the EdU labeling and the DAPI stain did not fully penetrate. In the work done by Fernández-Terán and colleagues (2006) quite uniform cell proliferation

was detected in the leg and foot paddle. In the data shown here we clearly see fewer proliferating cells in the center of the foot paddle (Figure 44). This area can be split into three more or less separate areas that fit well with the expected positions of the forming digits. Even though in the leg it is not completely guaranteed that the lack of labeled cells is due to insufficient penetration of the EdU, in the foot paddle there is no doubt that the EdU labeling worked as expected, as still a few labeled cells are visible within the areas of less cell proliferation.

At developmental stage HH28 the foot paddle showed areas with little cell proliferation, which in cross section show a ring-shaped pattern (Figure 49). Furthermore, in the leg two long and tube-shaped areas also showed only a little cell proliferation (Figure 50). In the study by Fernández-Terán et al. (2006) a similar and even more distinctive pattern was observed at HH29. Also at stage HH28 in their study, the proliferation looks more or less uniform within the limb, which does not fit together with the data shown here. This may result from the fact that only a selected cross section is shown and by that does not fully capture the pattern of the whole foot paddle.

Saunders and colleagues (1962) describe the INZ, as areas of cell death between the forming digits of chick embryos at stage HH31 in the forelimb. The same was reported by Fernández-Terán et al. (2006) in both the fore and hindlimb. This pattern was also observed in the data shown here, but especially in the midsection through the autopod (Figure 55). Moving just slightly away from that mid section, cell proliferation was still happening in the areas between the forming digits. This again shows that 3D data is essential to take proliferating cells like this into account when modeling for limb and digit development.

Cell apoptosis usually occurs in regions where forming skeletal elements are fused in the wrist or ankle, as well as in the autopod (Saunders Jr. et al., 1962). The data do show few proliferating cells in areas of forming skeletal elements or chondrogenesis, most obviously in areas where the DAPI stain shows the outline of the cartilage very nicely (see e.g. Figure 52Figure 53Figure 57). On the other hand, we still do see cell proliferation in the forming skeletal elements, for example in the digits (see e.g. Figure 51), at the epiphysis of the tibia (Figure 58), or where the joints in the forming digits are expected (Figure 55). Thus it seems

as though cell proliferation is less in these regions, but does not completely stop. In the data shown by Fernández-Terán et al. (2006) at stage HH31 and HH32, proliferating cells also were labeled both in the forming digits and at their outline. This again fits well with our data.

The fact that the data shown in this work corresponds well to the already known cell proliferation patterns confirms that our chosen method of fluorescent EdU chemistry does capture proliferating cells accurately. And doing so in 3D will add another dimension to understanding growing developing limbs. As chick embryos are often used as a model species in vertebrate limb development, the data is a valuable foundation for further research. It was shown that even with very simple computing cell densities can be illustrated based on the image data (Figure 61), and that cell counts can be conducted (Figure 60). These would enable, for example, the evaluation of the mitotic index in different areas of the limb, or the comparison and correlation of the imaged patterns with known and new gene expression patterns and signaling pathways (e.g. Fabre et al., 2018).

It is planned to publish an indexed set of the 3D image data and provide them to other interested researchers as an open-access resource, which will allow for easy inclusion in future projects (see Appendix, page 75). Understanding the normal distribution of proliferating cells is necessary as the basis to study deviations from it. The 3D files will be annotated and will consist of both the DAPI and Cy3 image sets for each developmental stage. It is noteworthy that in the early stages (HH18, HH20 and HH21) not only limbs but also the rest of the whole body was imaged (excluding the head) and in these cases also other areas besides the limbs could be analyzed if they are of interest.

Understanding how patterns and certain shapes develop is of great interest in biological research. Computer modeling can help to explore the boundaries and factors needed to achieve the formation of a certain structure or pattern, such as that of the vertebrate limb. On one hand the pattern produced by the skeletal elements in the limb is mostly explained by a self-organizing Turing pattern (Newman & Frisch, 1979; Raspopovic et al., 2014). In modeling morphogenesis in 3D, the vertebrate limb is one of the structures of interest

(Chaturvedi et al., 2005). The understanding of where and when cells proliferate will refine these models by ensuring that boundaries for the simulated cells can be set correctly.

This study contributes fundamental data to the documentation of the time course of growth during the development of limbs. These data can be used to guide future experiments that want to examine phenomena in limb development or want to manipulate them: knowing when and where to manipulate the tissue is crucial. One method to manipulate limb development is to place beads soaked in cell signaling proteins (e.g. FGF) or other solutions (e.g. retinoic acid) in certain areas and observe the emergence of morphological changes (see e.g. Bangs et al., 2010; Cohn et al., 1995). With the data produced in this work, not only the location of the manipulation can be estimated but also its timing in development.

The 3D images will be of most use in studies focusing on the growth and patterning of limbs, but do not limit it to these two topics. Just to name one other example, also evolutionary studies can profit from the data. Within this area, comparisons in a phylogenetic context will allow testing hypotheses about the roles of changing cell proliferation patterns in the evolution of different limb morphologies, such as digit origin, identity or reduction (de Bakker et al., 2013; Čapek et al., 2014; Saxena et al., 2017). Also, a comparison between species can be done, for example, with mice, which also are used in different limb development studies, focusing on for example gene expression and patterning of the skeletal elements (Ahn & Joyner, 2004; Benazet et al., 2009; Petit et al., 2017). Thus patterns specific for mammals or birds can be distinguished from a general vertebrate limb development pattern.

References

Ahn, S., & Joyner, A. L. (2004). Dynamic changes in the response of cells to positive Hedgehog signaling during mouse limb patterning. *Cell*, *118*(4), 505–516. https://doi.org/10.1016/j.cell.2004.07.023

de Bakker, M. A. G., Fowler, D. A., den Oude, K., Dondorp, E. M., Navas, M. C. G., Horbanczuk, J. O., et al. (2013). Digit loss in archosaur evolution and the interplay between selection and constraints. *Nature*, *500*, 445–8. https://doi.org/10.1038/nature12336

Bangs, F., Welten, M., Davey, M. G., Fisher, M., Yin, Y., Downie, H., et al. (2010). Identification of genes downstream of the Shh signalling in the developing chick wing and syn-expressed with Hoxd13 using microarray and 3D computational analysis. *Mechanisms of Development*, *127*, 428–441. https://doi.org/10.1016/j.mod.2010.08.001

Benazet, J.-D., Bischofberger, M., Tiecke, E., Goncalves, A., Martin, J. F., Zuniga, A., et al. (2009). A self-regulatory system of interlinked signaling feedback loops controls mouse limb patterning. *Science*, *323*(5917), 1050–1053. https://doi.org/10.1126/science.1168755

Bénazet, J.-D., & Zeller, R. (2009). Vertebrate Limb Development: Moving from Classical Morphogen Gradients to an Integrated 4-Dimensional Patterning System. *Cold Spring Harbor Perspectives in Biology*, *1*(a001339). https://doi.org/10.1101/cshperspect.a001339

Bolte, S., & Cordelières, F. P. (2006). A guided tour into subcellular colocalization analysis in light microscopy. *Journal of Microscopy*, *224*(3), 213–232. https://doi.org/10.1111/j.1365-2818.2006.01706.x

Čapek, D., Metscher, B. D., & Müller, G. B. (2014). Thumbs down: A molecular-morphogenetic approach to avian digit homology. *Journal of Experimental Zoology Part B: Molecular and Developmental Evolution*, *322B*, 1–12. https://doi.org/10.1002/jez.b.22545

Cappella, P., Gasparri, F., Pulici, M., & Moll, J. (2008). A novel method based on click chemistry, which overcomes limitations of cell cycle analysis by classical determination of BrdU incorporation, allowing multiplex antibody staining. *Cytometry Part A*, *73*(7),

626–636. https://doi.org/10.1002/cyto.a.20582

Chaturvedi, R., Huang, C., Kazmierczak, B., Schneider, T., Izaguirre, J. A., Glimm, T., et al. (2005). On multiscale approaches to three-dimensional modelling of morphogenesis. *Journal of the Royal Society Interface*, *2*(3), 237–253. https://doi.org/10.1098/rsif.2005.0033

Chazotte, B. (2011). Labeling nuclear DNA using DAPI. *Cold Spring Harbor Protocols*, pdb.prot5556. https://doi.org/10.1101/pdb.prot5556

Chehrehasa, F., Meedeniya, A. C. B., Dwyer, P., Abrahamsen, G., & Mackay-Sim, A. (2009). EdU, a new thymidine analogue for labelling proliferating cells in the nervous system. *Journal of Neuroscience Methods*, *177*(1), 122–130. https://doi.org/10.1016/j.jneumeth.2008.10.006

Cohn, M. J., Izpisúa-Belmonte, J. C., Abud, H., Heath, J. K., & Tickle, C. (1995). Fibroblast growth factors induce additional limb development from the flank of chick embryos. *Cell*, *80*(5), 739–746. https://doi.org/10.1016/0092-8674(95)90352-6

Drossopoulou, G., Lewis, K. E., Sanz-Ezquerro, J. J., Nikbakht, N., McMahon, a P., Hofmann, C., & Tickle, C. (2000). A model for anteroposterior patterning of the vertebrate limb based on sequential long- and short-range Shh signalling and Bmp signalling. *Development*, *127*, 1337–1348.

Ede, D. A., Flint, O. P., & Teague, P. (1975). Cell proliferation in the developing wing-bud of normal and talpid3 mutant chick embryos. *Journal of Embryology and Experimental Morphology*, *34*(3), 589–607. Retrieved from http://www.ncbi.nlm.nih.gov/pubmed/1214111

Fabre P. J., Leleu M., Mascrez B., Lo Giudice Q., Cobb J., & Duboule D. (2018). Heterogeneous combinatorial expression of Hoxd genes in single cells during limb development. *BMC Biology,* 16(1), 101. Retrieved from http://www.ncbi.nlm.nih.gov/pmc/articles/PMC6142630/

Fallon, J. F., López, A., Ros, M. A., Savage, M. P., Olwin, B. B., & Simandl, B. K. (1994). FGF-2: Apical ectodermal ridge growth signal for chick limb development. *Science*, *264*(5155), 104–107. https://doi.org/10.1126/science.7908145

Fell, H. B., & Canti, R. G. (1934). Experiments on the development in vitro of the avian knee-joint. *Proceedings of the Royal Society B: Biological Sciences*, *116*(799), 316–351. https://doi.org/10.1098/rspb.1934.0076

Fernández-Terán, M. A., Hinchliffe, J. R., & Ros, M. A. (2006). Birth and death of cells in limb development: A mapping study. *Developmental Dynamics*, *235*, 2521–2537. https://doi.org/10.1002/dvdy.20916

Glimm, T., Bhat, R., & Newman, S. A. (2014). Modeling the morphodynamic galectin patterning network of the developing avian limb skeleton. *Journal of Theoretical Biology*, *346*, 86–108. https://doi.org/10.1016/j.jtbi.2013.12.004

Green, J. B. A., & Sharpe, J. (2015). Positional information and reaction-diffusion: two big ideas in developmental biology combine. *Development*, *142*, 1203–1211. https://doi.org/10.1242/dev.114991

Hamburger, V., & Hamilton, H. L. (1951). A series of normal stages in the development of the chick embryo. *Journal of Morphology*, *88*(3), 49–92. https://doi.org/10.1002/aja.1001950404

Hentschel, H. G. E., Glimm, T., Glazier, J. A., & Newman, S. A. (2004). Dynamical mechanisms for skeletal pattern formation in the vertebrate limb. *Proceedings of the Royal Society B: Biological Sciences*, *271*, 1713–1722. https://doi.org/10.1098/rspb.2004.2772

Hinchliffe, J. R., & Thorogood, P. V. (1974). Genetic inhibition of mesenchymal cell death and the development of form and skeletal pattern in the limbs of talpid3 (ta3) mutant chick embryos. *Journal of Embryology and Experimental Morphology*, *31*(3), 747–60. Retrieved from http://www.ncbi.nlm.nih.gov/pubmed/4448949

Hiraoka, T., & Hirai, K.-I. (1992). Platinum-Diaminobenzidine Reaction and Its Contribution to the Ouantitation of Cytochrome Oxidase Activity. *Journal of Electron Microscopy*, *41*, 127–129.

Hiscock, T. W., Tschopp, P., & Tabin, C. J. (2017). On the formation of digits and joints during limb development. *Developmental Cell*, *41*(5), 459–465. https://doi.org/10.1016/j.devcel.2017.04.021

Hornbruch, A., & Wolpert, L. (1970). Cell division in the early growth and morphogenesis of the chick limb. *Nature*, *226*, 764–766. https://doi.org/10.1038/226764a0

Jonkman, J., & Brown, C. M. (2015). Any way you slice it - A comparison of confocal microscopy techniques. *Journal of Biomolecular Techniques*, *26*(2), 54–65. https://doi.org/10.7171/jbt.15-2602-003

Kawakami, Y., Capdevila, J., Büscher, D., Itoh, T., Esteban, C. R., & Belmonte, J. C. I. (2001). WNT signals control FGF-dependent limb initiation and AER induction in the chick

embryo. *Cell*, *104*(6), 891–900. https://doi.org/10.1016/S0092-8674(01)00285-9

Kondo, S. (2009). How animals get their skin patterns: fish pigment pattern as a live Turing wave. In S. Nakanishi, R. Kageyama, & D. Watanabe (Eds.), *Systems Biology* (pp. 37–46). Tokyo: Springer Japan.

Mariani, F. V., Fernandez-Teran, M., & Ros, M. A. (2017). Ectoderm–mesoderm crosstalk in the embryonic limb: The role of fibroblast growth factor signaling. *Developmental Dynamics*, *246*(4), 208–216. https://doi.org/10.1002/dvdy.24480

Marin-Riera, M., Brun-Usan, M., Zimm, R., Välikangas, T., & Salazar-Ciudad, I. (2016). Computational modeling of development by epithelia, mesenchyme and their interactions: a unified model. *Bioinformatics*, *32*(2), 219–225. https://doi.org/10.1093/bioinformatics/btv527

Meinhardt, H. (2008). Models of biological pattern formation: from elementary steps to the organization of embryonic axes. *Current Topics in Developmental Biology*, *81*, 1–63. https://doi.org/10.1016/S0070-2153(07)81001-5

Metscher, B. D. (2009). MicroCT for developmental biology: A versatile tool for high-contrast 3D imaging at histological resolutions. *Developmental Dynamics*, *238*, 632–640. https://doi.org/10.1002/dvdy.21857

Metscher, B. D., & Müller, G. B. (2011). MicroCT for Meolecular Imaging: Quantitative Visualization of Complete Three-Dimensional Distributions of Gene Products in Embryonic Limbs. *Developmental Dynamics*, *240*, 2301–2308. https://doi.org/10.1002/dvdy.22783

Müller, G. B. (2007). Evo-devo: extending the evolutionary synthesis. *Nature Reviews Genetics*, *8*, 943–949. Retrieved from http://www.hup.harvard.edu/catalog.php?isbn=9780674865389

Newman, G. R., Jasani, B., & Williams, E. D. (1983). Metal Compounf Intesification of the Electron-density of Diaminobenzidine. *The Journal of Histochemistry and Cytochemistry*, *31*(12), 1430–1434.

Newman, S. A., & Frisch, H. L. (1979). Dynamics of skeletal pattern formation in developing chick limb. *Science*, *205*(4407), 662–668. https://doi.org/10.1126/science.462174

Niswander, L. (2003). Pattern formation: old models out on a limb. *Nature Reviews Genetics*, *4*, 133–143. https://doi.org/10.1038/nrg1001

Petit, F., Sears, K. E., & Ahituv, N. (2017). Limb development: A paradigm of gene regulation.

Nature Reviews Genetics, *18*, 245–258. https://doi.org/10.1038/nrg.2016.167

Raspopovic, J., Marcon, L., Russo, L., & Sharpe, J. (2014). Digit patterning is controlled by a Bmp-Sox9-Wnt Turing network modulated by morphogen gradients. *Science*, *345*(6196), 566–570. https://doi.org/10.1126/science.1252960

Rostovtsev, V. V, Green, L. G., Fokin, V. V, & Sharpless, K. B. (2002). A Stepwise Huisgen Cycloaddition Process: Copper(I)-Catalyzed Regioselective "Ligation" of Azides and Terminal Alkynes. *Angewandte Chemie - International Edition*, *41*(14), 2596–99. https://doi.org/10.1021/jo011148j

Salic, A., & Mitchison, T. J. (2008). A chemical method for fast and sensitive detection of DNA synthesis in vivo. *Proceedings of the National Academy of Sciences of the United States of America*, *105*(7), 2415–20. https://doi.org/10.1073/pnas.0712168105

Saunders Jr., J. W. (1984). The proximo-distal sequence of origin of the parts of the chick wing and the role of the ectoderm. *Journal of Experimental Zoology*, *108*(3), 363–403.

Saunders Jr., J. W., Gasseling, M. T., & Saunders, L. C. (1962). Cellular death in morphogenesis of the avian wing. *Developmental Biology*, *5*, 147–178.

Saxena, A., Towers, M., & Cooper, K. L. (2017). The origins, scaling and loss of tetrapod digits. *Philosophical Transactions of the Royal Society of London B: Biological Sciences*, *372*(1713). https://doi.org/10.1098/rstb.2015.0482

Sharpe, J. (2002). Optical Projection Tomography as a Tool for 3D Microscopy and Gene Expression Studies. *Science*, *296*(5567), 541–545. https://doi.org/10.1126/science.1068206

Sharpe, J. (2004). Optical projection tomography. In C. W. Sensen & B. Hallgrímsson (Eds.), *Advanced Imaging in Biology and Medicine: Technology, Software Environments, Applications* (pp. 199–224). Springer, Berlin, Heidelberg. https://doi.org/10.1007/978-3-540-68993-5_9

Sharpe, J., Ahlgren, U., Perry, P., Hill, B., Ross, A., Hecksher-Sørensen, J., et al. (2002). Optical projection tomography as a tool for 3D microscopy and gene expression studies. *Science*, *296*(5567), 541–545. https://doi.org/10.1126/science.1068206

Shubin, N., Tabin, C., & Carroll, S. (1997). Fossils, genes and the evolution of animal limbs. *Nature*, *388*, 639–48. https://doi.org/10.1038/41710

Sun, X., Mariani, F. V., & Martin, G. R. (2002). Functions of FGF signalling from the apical ectodermal ridge in limb development. *Nature*, *418*(6897), 501–508.

https://doi.org/10.1038/nature00902

Susaki, E. A., Tainaka, K., Perrin, D., Kishino, F., Tawara, T., Watanabe, T. M., et al. (2014). Whole-brain imaging with single-cell resolution using chemical cocktails and computational analysis. *Cell*, *157*(3), 726–739. https://doi.org/10.1016/j.cell.2014.03.042

Tainaka, K., Kubota, S. I., Suyama, T. Q., Susaki, E. A., Perrin, D., Ukai-Tadenuma, M., et al. (2014). Whole-body imaging with single-cell resolution by tissue decolorization. *Cell*, *159*(4), 911–924. https://doi.org/10.1016/j.cell.2014.10.034

Tickle, C., & Eichele, G. (1994). Vertebrate Limb Development. *Annual Review of Cell Biology*, *10*(1), 121–152. https://doi.org/10.1146/annurev.cb.10.110194.001005

Tickle, C., & Towers, M. (2017). Sonic Hedgehog Signaling in Limb Development. *Frontiers in Cell and Developmental Biology*, *5*(14). https://doi.org/10.3389/fcell.2017.00014

Tickle, C., Summerbell, D., & Wolpert, L. (1975). Positional signalling and specificiation of digits in chick limb morphogenesis. *Nature*, *254*, 199–202. https://doi.org/10.1038/253600a0

Tornøe, C. W., Christensen, C., & Meldal, M. (2002). Peptidotriazoles on Solid Phase: [1,2,3]-Triazoles by Regiospecific Copper(I)-Catalyzed 1,3-Dipolar Cycloadditions of Terminal Alkynes to Azides. *The Journal of Organic Chemistry*, *67*(9), 3057–3064. https://doi.org/10.1021/jo011148j

Towers, M. (2018). Evolution of antero-posterior patterning of the limb: Insights from the chick. *Genesis*, *56*(1), e23047. https://doi.org/10.1002/dvg.23047

Turing, A. M. (1952). The chemical basis of morphogenesis. *Philosophical Transactions of the Royal Society B*, *237*, 37–72.

Wagner, G. P., & Chiu, C.-H. (2001). The tetrapod limb: A hypothesis on its origin. *Journal of Experimental Zoology*, *291*(3), 226–240. https://doi.org/10.1002/jez.1100

Wang, S., & Larina, I. V. (2017). High-resolution imaging techniques in tissue engineering. In R. J. Narayan (Ed.), *Monitoring and Evaluation of Biomaterials and their Performance In Vivo* (pp. 151–180). Woodhead Publishing.

Warren, M., Puskarczyk, K., & Chapman, S. C. (2009). Chick embryo proliferation studies using EdU labeling. *Developmental Dynamics*, *238*, 944–949. https://doi.org/10.1002/dvdy.21895

Wong, M. D., Dazai, J., Walls, J. R., Gale, N. W., & Henkelman, R. M. (2013). Design and

Implementation of a Custom Built Optical Projection Tomography System. *PLoS ONE*, *8*(9), e73491. https://doi.org/10.1371/journal.pone.0073491

Yokoyama, S., Furukawa, S., Kitada, S., Mori, M., Saito, T., Kawakami, K., et al. (2017). Analysis of transcription factors expressed at the anterior mouse limb bud. *PLoS ONE*, *12*(5), e0175673. https://doi.org/10.1371/journal.pone.0175673

Zakeri, Z. F., Quaglino, D., Latham, T., & Lockshin, R. A. (1993). Delayed internucleosomal DNA fragmentation in programmed cell death. *The FASEB Journal*, *7*, 470–78.

Zhu, J., Zhang, Y. T., Alber, M. S., & Newman, S. A. (2010). Bare bones pattern formation: A core regulatory network in varying geometries reproduces major features of vertebrate limb development and evolution. *PLoS ONE*, *5*(5), e10892. https://doi.org/10.1371/journal.pone.0010892

Appendix

Index of Image Data

Stage HH18

…/HH18_Cy3_forelimb.zip, Voxel size: 0.914x0.914x4.876µm, 4.42GB

…/HH18_DAPI_forelimb.zip, Voxel size: 0.914x0.914x4.876µm, 4.42GB

…/HH18_Cy3_hindlimb.zip, Voxel size: 0.914x0.914x4.876µm, 9.55GB

…/HH18_DAPI_hindlimb.zip, Voxel size: 0.914x0.914x4.876µm, 9.55GB

Stage HH20

…/HH20_Cy3_bothlimbs.zip, Voxel size: 0.914x0.914x4.876µm, 13.3GB

…/HH20_DAPI_bothlimbs.zip, Voxel size: 0.914x0.914x4.876µm, 13.3GB

…/HH20_Cy3_bothlimbs_reduced.zip, Voxel size: 1.827x1.827x9.752µm, 2.42GB

…/HH20_DAPI_bothlimbs_reduced.zip, Voxel size: 1.827x1.827x9.752µm, 2.42GB

Stage HH21

.../HH21_Cy3_bothlimbs.zip, Voxel size: 0.914x0.914x4.802µm, 19.4GB

.../HH21_DAPI_bothlimbs.zip, Voxel size: 0.914x0.914x4.802µm, 19.4GB

…/HH21_Cy3_bothlimbs_reduced.zip, Voxel size: 1.827x1.827x9.604µm, 2.42GB

…/HH21_DAPI_bothlimbs_reduced.zip, Voxel size: 1.827x1.827x9.604µm, 2.42GB

Stage HH25-

…/HH25-_Cy3_forelimb.zip, Voxel size: 1.305x1.305x3.996µm, 3.47GB

…/HH25-_DAPI_forelimb.zip, Voxel size: 1.305x1.305x3.996µm, 3.47GB

…/HH25-_Cy3_hindlimb.zip, Voxel size: 1.305x1.305x3.996µm, 4.3GB

…/HH25-_DAPI_hindlimb.zip, Voxel size: 1.305x1.305x3.996µm, 4.3GB

…/HH25-_Cy3_bothlimbs.zip, Voxel size: 1.305x1.305x3.996µm, 62.8GB

…/HH25-_DAPI_bothlimbs.zip, Voxel size: 1.305x1.305x3.996µm, 62.8GB

Stage HH25

…/HH25_Cy3_forelimb.zip, Voxel size: 0.761x0.761x4.802µm, 38.3GB

…/HH25_DAPI_forelimb.zip, Voxel size: 0.761x0.761x4.802µm, 38.3GB

…/HH25_Cy3_forelimb_reduced.zip, Voxel size: 1.523x1.523x9.604µm, 4.78GB

…/HH25_DAPI_forelimb_reduced.zip, Voxel size: 1.523x1.523x9.604µm, 4.78GB

…/HH25_Cy3_hindlimb.zip, Voxel size: 0.761x0.761x4.802µm, 22.1GB

…/HH25_DAPI_hindlimb.zip, Voxel size: 0.761x0.761x4.802µm, 22.1GB

…/HH25_Cy3_hindlimb_reduced.zip, Voxel size: 1.523x1.523x9.604µm, 2.76GB

…/HH25_DAPI_hindlimb_reduced.zip, Voxel size: 1.523x1.523x9.604µm, 2.76GB

Stage HH26-

…/HH26-_Cy3_forelimb.zip, Voxel size: 0.914x0.914x4.876µm, 24.2GB

…/HH26-_DAPI_forelimb.zip, Voxel size: 0.914x0.914x4.876µm, 24.2GB

…/HH26-_Cy3_forelimb_reduced.zip, Voxel size: 1.827x1.827x9.753µm, 3.02GB

…/HH26-_DAPI_forelimb_reduced.zip, Voxel size: 1.827x1.827x9.753µm, 3.02GB

Stage HH27-

…/HH27-_Cy3_hindlimb.zip, Voxel size: 0.914x0.914x4.876µm, 10.4GB

…/HH27-_DAPI_hindlimn.zip, Voxel size: 0.914x0.914x4.876µm, 10.4GB

Stage HH28

…/HH28_Cy3_hindlimb.zip, Voxel size: 0.914x0.914x4.844µm, 16GB

…/HH28_DAPI_hindlimb.zip, Voxel size: 0.914x0.914x4.844µm, 16GB

…/HH28_Cy3_hindlimb_reduced.zip, Voxel size: 1.827x1.827x9.688µm, 2GB

…/HH28_DAPI_hindlimb_reduced.zip, Voxel size: 1.827x1.827x9.688µm, 2GB

Stage HH31

…/HH31_Cy3_forelimb.zip, Voxel size: 0.914x0.914x4.844µm, 18GB

…/HH31_DAPI_forelimb.zip, Voxel size: 0.914x0.914x4.844µm, 18GB

…/HH31_Cy3_hindlimb.zip, Voxel size: 0.914x0.914x4.876µm, 34.7GB

…/HH31_DAPI_hindlimb.zip, Voxel size: 0.914x0.914x4.876µm, 34.7GB

…/HH31_Cy3_forelimb_reduced.zip, Voxel size: 1.827x1.827x9.688µm, 2.24GB

…/HH31_DAPI_forelimb_reduced.zip, Voxel size: 1.827x1.827x9.688µm, 2.24GB

…/HH31_Cy3_hindlimb_reduced.zip, Voxel size: 1.827x1.827x9.753µm, 4.33GB

…/HH31_DAPI_hindlimb_reduced.zip, Voxel size: 1.827x1.827x9.753µm, 4.33GB